Design of a Mechanical Failure Criterion for Living Human Tissue

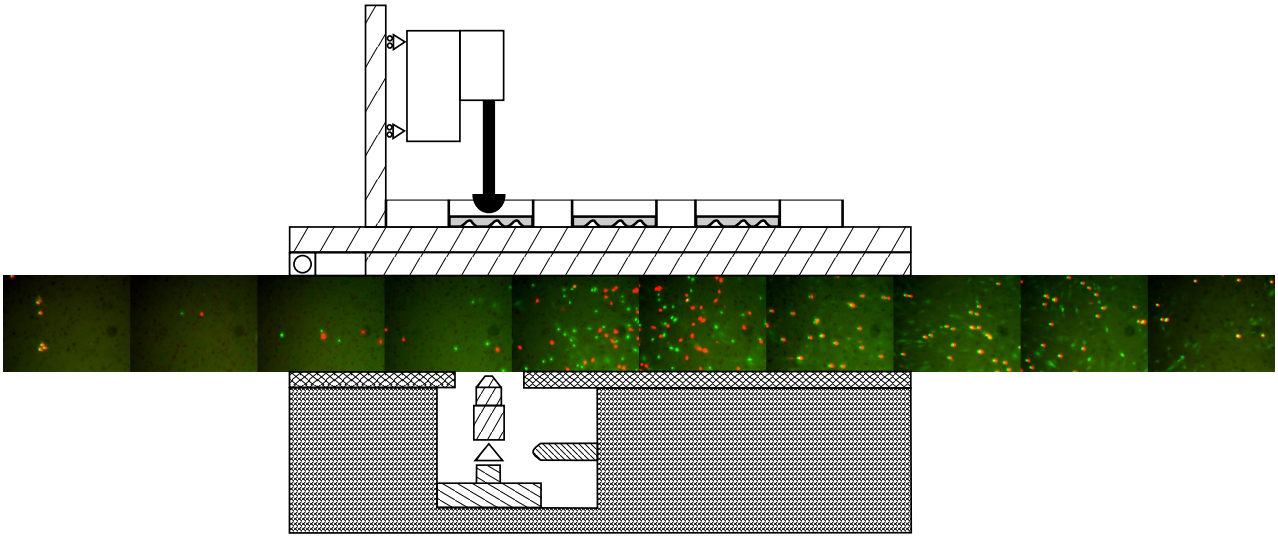

Design of Mechanical Systems

10^{th} Semester Master's Thesis

June 2017

Daniel S. Gibson

Institut for Mekanik og Produktion
Maskin og Produktion
Fibigerstræde 16, 9220 Aalborg
Telefon 99 40 71 17
Fax 99 40 71 10
http://info@m-tech.aau.dk

Title:

Design of a Mechanical Failure Criterion for Living Human Tissue

Theme:

Bio-mechanical Engineering

Project duration:

DMS10, Spring Semester 2017

Authors:

Daniel Sean Gibson

Supervisor:

John Rasmussen

Cristian Pablo Pennisi

Hand-in date: 02.06.2017

Synopsis:

This thesis is concerned with the effects of mechanical loading on living human tissue cells so as to progress towards developing a mechanical failure criterion for living human tissue.

An existing experimental set-up was further developed and four experiments were run with an aim of investigating the effects of strain on the rate of change of cell viability.

Overall, the results demonstrated that there was a significant impact of mechanical loads on cell viability, however, further testing needs to be undertaken to provide more data on the effects of strain state on cell death.

Preface

This master's thesis is the result of work carried out on the 10^{th} semester of the 'Design of Mechanical Systems' curriculum as part of the Department of Mechanical Engineering, Aalborg University, Denmark. The work has been carried out in partial fulfilment of the requirements for the Master of Science degree. The report has been supervised by Prof. John Rasmussen and Prof. Cristian Pablo Pennisi.

The title of the report is:

Design of a Mechanical Failure Criterion for Living Human Tissue

The report consists of a main report.

Citations are done in accordance with the Harvard Style. This is the authors own work.
Aalborg University, June 2017
Daniel S. Gibson

Acknowledgements

Special thanks must go to Prof. John Rasumussen and Prof. Cristian Pablo Pennisi for all of their support and knowledge. I enjoyed working on this project with you and learnt more than I ever could have expected.

Abstract

Numerous diseases are related to the breaking down of muscle tissues due to the effects of mechanical loading. Deep tissue pressure ulcers (PU) are one such disease that have a significant cost to patient welfare and high financial costs due to patient care and treatment. The disease can be difficult to detect until it reaches a severe state and is difficult to treat.

A time-lapse experiment has previously been developed by Aalborg University alumni to investigate the effects of strain state on the rate of change of cell viability. The overall aim of the experiment is to develop a mechanical failure criterion for living human tissue. It is believed that through continued investigation into the effects of strains, specifically, shear strains, on living human tissue cells, evidence-based intervention methods can be put into place to reduce the risk of associated diseases.

The experimental procedure captures image sequences to investigate the effects of strain on living tissue samples. A specially designed aluminium indenter is used to apply a load to the centre of a cell sample and the effects over a relatively large area are observed by capturing a sequence of images. The observations are repeated at regular time intervals over a period of approximately eight hours, as well as after twenty hours. The number of dead cells observed through cell staining techniques.

This thesis documents the processes that have been undertaken to further develop the experimental set-up. Four experiments were undertaken and the results have suggested that mechanical loading has a significant effect on cell viability. Further work is needed to develop this. Of the four experiments undertaken, three of the experiments suffered from exposure problems or sparse cell samples which made the analysis processes difficult. The fourth experiment fixed all of these problems but was terminated prematurely due to a mechanical failure. Despite this, the experiments have demonstrated that, with some small refinements, the methods used in this thesis will be suitable for developing a mechanical failure criterion for living human tissue.

Resumé

Adskillige sygdomme er forbundet med nedbrydning af muskelvæv på grund af mekaniske belastninger. Tryksår er en af disse sygdomme, som medfører en betydelig omkostning for patienten i form af tabt livskvalitet og for samfundet i form af høje omkostninger til behandling.

Tryksår i de dybe væv er vanskelige at detektere, før de når et kritisk stadium og er vanskelige at behandle.

Et time-lapse-eksperiment er tidligere udført på Aalborg Universitet til undersøgelse af effekterne af tøjningstilstanden på cellers overlevelse. Det overordnede mål med dette eksperiment er at udvikle et mekanisk fejlkriterium for levende menneskeligt væv. Det antages, at fortsatte eksperimenter med effekten af tøjning, specielt forskydningstøjning, på levende humane celler, kan føre til udvikling af evidensbaserede interventioner, som kan reducere risikoen for udvikling af de tilhørende sygdomme.

Formålet med eksperimentet er at optage billeder for at undersøge effekten af tøjning på levende vævsprøver. Et specielt designet aluminiumsstempel bruges til at påtrykke belastning i centrum af en celleprøve, og effekten over et relativt stort område observeres ved at optage en sekvens af billeder. Observationerne gentages med ensartede tidsintervaller over en periode på ca. otte timer, og efter 20 timer. Antallet af døde celler registreres ved hjælpe af staining-teknikker.

Denne rapport dokumenterer processerne, der er gennemført til videre udvikling af eksperimentet.

Table of contents

List of Figures

Chapter 1

Introduction

The interaction between mechanical loading and the growth and propagation of living tissue is a well investigated field. Increasingly, research has been concerned with the effects of mechanical loading on the breaking down of living human tissue; what are the causes and mechanisms that cause tissue failure under the impact of loading? This field is of much significance to research due to the fact that there are numerous diseases associated with the mechanical breaking down of tissue; the cardiac, skeletal and soft muscle tissue systems have severe diseases which propagate due to loading.

Pressure ulcers are one such disease that are onset by sustained mechanical loading and can either affect the skin or the underlying tissue, typically around bony areas and joints. Pressure ulcers can be divided into superficial and deep tissue classifications. Superficial pressure ulcers are visible and are caused by breaking down of skin tissues. Deep tissue pressure ulcers are almost undetectable until there has been a severe breakdown in internal tissues. The latter form of pressure ulcer are extremely difficult to treat, are extremely painful and have high treatment costs. According to the English National Health Service, pressure ulcer treatment costs between £ 1.4 - £ 2.1 billion annually; a cost that accounts for 4% of the annual expenditure [Bennett et al., 2004]. The problem is so prevalent that in February 2016, the NHS hosted the North Region Pressure Ulcer Summit to try and raise awareness to the problems facing high risk patients. These patients are typically bed ridden patients, such as paralysis victims. In these cases the soft tissue systems can be subjected to sustained pressures over long periods of time.

There have been many different considerations as to the reasons that pressure ulcers propagate. These include:

- Sustained cell deformation - cells are subjected to loading causing deformation of their cell membranes. This leads to tissue breakdown which causes pressure ulcers to propagate. There are numerous considerations as to why cells die when subjected to loading such as damage caused to the cytoskeleton and permeability changes to the plasma wall.
- Localised Ischemia - where the blood supply to localised tissue is blocked; this reduces the amount of oxygen that can be absorbed by the tissue which leads to lactic acid poisoning
- Ischemia-reperfusion injury - when blood returns to regions that have suffered from ischemia. Some studies have demonstrated that muscle tissue is able to sustain long periods of ischemia but is far more susceptible to damage from iscemia-reperfusion injury ([Hoek et al., 1996])

Although there are many considerations as to what mechanism causes tissue to breakdown due to loading, it is agreed that tissue failure initiates the onset of pressure ulcers. In material

sciences, mechanical failure criterion are used to predict the point at which a material will fail when subjected to loading. By applying some of the core concepts of material mechanics to living tissue it should be possible to gain a statistical, materialistic understanding of how tissue behaves under loading. This information could then be used as an insight into how to prevent diseases that are related to tissue failure due to loading. It is thought that by creating a mechanical failure criterion for living human tissue, evidence based intervention methods could be established to help prevent the onset of the disease.

In order to fully understand the mechanisms behind tissue breakdown, a literature review will be conducted. The purpose of this is to understand what methods cause tissue breakdown and how other studies have been conducted.

1.1 Literature Review

Numerous studies have been undertaken to investigate the effects of mechanical loading on living cells and have determined that sustained mechanical loading can have a negative impact on cell health. [Bouten et al., 2001] and [Breuls et al., 2003] performed similar experiments which demonstrated that cell deformation had significant effects on cell viability.

[Bouten et al., 2001] performed an experiment to investigate the effects of compressive straining on muscle cell deformation and damage. The cells were subjected to a sustained linear compressive strain; deformation was measured by in-plane orthogonal diameter measurements of the cell before and after straining whilst cell damage was assessed by investigating membrane disruption and nucleus fragmentation. It was found that cell damage was considerably higher in cell samples that were subjected to a continuous 20% compressive straining compared to unstrained samples.

Similarly, an experiment was performed by [Breuls et al., 2003], however, cell compression was initiated by indenting cells with a rod-like indenter of circular cross-section with a flat surface. Unlike [Bouten et al., 2001], damage to the sample was assessed by monitoring cell viability, however, the results were the same. It was found that cell samples that were subjected to sustained compressive strains of 30% and 50% for eight hours had a higher level of damage in comparison to uncompressed samples. In this experiment, strain was considered to be a linear parameter.

Whilst these studies have suggested that cell straining has an impact on cell damage, the mechanisms that cause cell death are still being investigated. The sustained cell deformation theory suggests that deformation is a more important factor in cell health than hypoxia. This has been supported by [Gawlitta et al., 2006] yet the causes at a cellular level remained undetermined.

Ceelen2009 hypothesised that damage was caused to the cells by an influx of calcium ions, Ca^{2+}, due to permeability changes in deformed cells. An experiment was devised but the results were inconclusive. Despite this, supportive evidence exists in the form of a computer model which suggested that large cell deformations could increase the Ca^{2+} influx [Slomka and Grefen, 2010].

This is supported by numerous studies have been conducted over the last ten years into the consequences of sustained (non-lethal) tensile strains on the permeability of myoblast cells. These studies were undertaken specifically for investigations into the onset of pressure ulcers.

It was found that applying strains of between 3-12% to the cell's plasma membrane significantly increased permeability to the membrane itself. The overall conclusion was that cell deformation itself was responsible for the onset of deep tissue pressure ulcers and indicated that further study was needed in this field [Gefen et al., 2008], [Leopold and Geffen, 2013] and [Slomka and Gefen, 2012].

1.2 Overview of Previous Work

The present investigation is a continuation of the work undertaken by AAU alumni [Rasmussen, 2013], [da Silva Ferreira, 2014] and [Gibson, 2016].

A mechanical experiment has been devised to investigate the effects of compressive loading on the rate of change of cell viability. [Rasmussen, 2013] documents the initial experimental set-up as well as developing a specialised alginate gel which is used to immobilise the cells and to transfer the stresses imposed by a mechanical indenter to the cells.

[da Silva Ferreira, 2014] developed cell staining techniques which were used to signal whether a cell was alive or dead; a key component of the experiment. His work validated the theory that the experiment was appropriate for investigating the effects of strain state on the rate of change of cell viability and obtained initial results which suggested that mechanical loading made a significant impact on the rate of cell viability.

[Gibson, 2016] developed the overall experiment with a view to automating many of the key processes needed as part of the experiment. The aim was to develop the experiment so that it would be easier to obtain the large quantity of data that would be needed to develop a mechanical failure criterion, as well as to improve the accuracy and repeatability of the experiment.

In summary, an experiment has been developed to investigate the effects of strain on the rate of change of cell viability. The existing documentation can be referred to for clarity where necessary and serves as a historical reference that documents the entirety of the project, from initiation to the current point.

Where required, essential information will be documented in this report for clarity and the original documentation will be referenced.

Chapter 2

Thesis Outline

The aim of the project is to determine a mechanical failure criterion for living human tissue. The thesis aim and objectives will be documented here with a view to pushing the project closer to achieving the overall project aim.

2.1 Thesis Aims and Objectives

The aim of this thesis is to investigate the effects of mechanical loading on the rate of change of cell viability. In order to do this the following objectives need to be achieved:

- Obtaining data by performing a series of experiments on living human tissue cells using the experimental set up as developed by [Rasmussen, 2013], [da Silva Ferreira, 2014] and [Gibson, 2016]. This includes developing the experiment so that it is better suited for capturing the large-scale effects of loading, preparing the experiment and fabricating any materials that are necessary.
- Either manually or automatically analysing the data. If an automatic method is selected then an 'in-house' method should be developed or a viable commercial alternative should be found.
- Initial steps should be taken to develop a mechanical failure criterion. This includes researching various existing mechanical failure criterion and using these to determine how certain features could be applied to living human tissue.

Moreover, there are some additional objectives. These are not required to complete the thesis but would improve the overall experimental process. The additional objectives include:

- Implement and develop the existing numerical model and use this as a reference for the strain distribution in the cell sample.
- Further, the material investigations for alginate gels as undertaken by [Rasmussen, 2013]
- Developing a fully automatic experiment by furthering the work achieved by [Gibson, 2016]. This would include developing an autofocus system for the microscope and developing an 'in-house' analysis software which is specifically designed for this experiment.

Chapter 3

Theory

This thesis is concerned with the effects of mechanical loading on living human tissue cells with a view to producing a mechanical failure criterion in the future. The following chapter will be used to introduce the necessary basics of the mechanics of a cell, material mechanics, and a background of mechanical failure criteria.

3.1 Introduction to Cell Mechanics and Behaviour

To investigate the effects of mechanical loading on living human tissue, it imperative that an understanding of the mechanics of living cells is understood. Living tissues behave dynamically in the fact that they respond to loading by changing its shape, size and cellular structure. Moreover, the mechanical and material properties of a cell can change over time.

Even at a cellular level, tissues are complex composite structures, which makes them especially difficult to describe theoretically. What is known, is that cells display both elastic and viscous effects, which, will need to be taken into account for any description of a cell and its mechanical behaviour.

Cells are composed of three primary elements; the cell membrane, the cytoplasm and the nucleus. Cells that contain these three elements are called eukaryote cells.

The cell membrane of a eukaryote cell is approximately (10nm) thick and it acts a barrier between the cells interior and the outside world. The membrane is constructed of lipids and proteins and is a selective, permeable barrier.

The cytoplasm is the name of any part of the internal structure of a cell, not including the nucleus and includes the cytoskeleton ad the cytosol.

The nucleus in separated from the cytoplasm by a nuclear envelope. The purpose of the nucleus is to store the genetic make-up of the cell and to control cell functions such as growth and metabolism.

The nucleus is up to four times stiffer and twice as viscous as the cytoplasm.

Myoblast cells are typically used for deformations studies. These can be differentiated to create muscle tissues.

3.2 Introduction to Mechanics of Materials

Material behaviour and mechanics is a broad topic with multiple disciplines, variations and approaches and as such it will only be touched upon here to introduce the reader to the basic concepts as well as the notation used throughout this thesis. There are numerous books and learning materials that can be found for further reading, however, much of the following section will be based on [Dym and Shames, 2013]. The purpose of this section is to demonstrate how stresses and strains are distributed and derived at all points within a body. The section should also demonstrate that both stress and strain are tensor quantities

3.2.1 Stress

The study of material mechanics is primarily concerned with the distribution of forces through a body and the effects that the forces have on the body. There are two categories of forces that will be focused on within this section; body forces and surface tractions. Body forces act directly throughout the matter of the body and is an intensity function evaluated over the volume of a body. It is donated as a function of space and time $B(x, y, z, t)$ but will be represented in index notation as $B_i(x_1, x_2, x_3, t)$. Surface tractions are forces that act over the boundary of a structure, typically this boundary would be the surface of a structure, however, it could also be over a mathematically imposed boundary. Surface tractions are also intensity functions, they are evaluated over areas. Again, traction forces are functions of space and time and denoted as $T(x, y, z, t)$ and can be referenced in index notation $T_i(x_1, x_2, x_3, t)$.

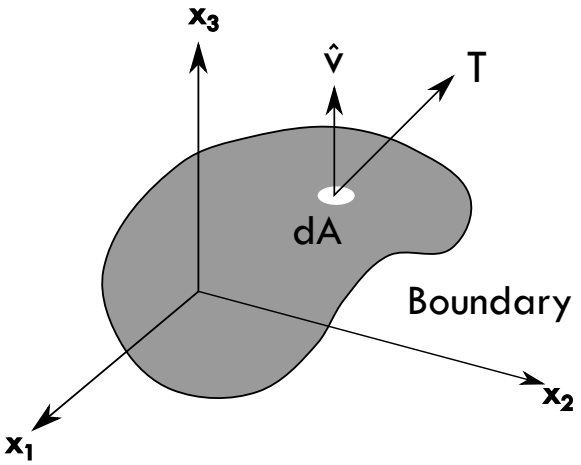

Figure 3.1: An infinitesimal area taken on the surface of a body. The unit normal and traction vector with arbitrary direction are shown

In Fig. 3.1 a body is shown with an infinitesimal area taken on the boundary over which a surface traction, T, acts. The force, df_i transmitted across the area is given by:

$$df_i = T_i dA$$

Fig. 3.1 has the unit normal for the area shown, $\hat{v}$, this serves to illustrate that the surface traction need not act parallel to or in the direction of the unit normal. The unit normal is also necessary to express on what area of a body the traction is acting over and will be added to the notation of the tractions as a superscript:

$$T_i^{(v)}(x_1, x_2, x_3, t)$$

This means that it is possible to identify tractions acting on different surfaces of a body.
An infinitesimal rectangular parallelepiped is considered to be taken at a point from within the body shown in Fig. 3.1 and is assigned a reference frame with axis x_1, x_2 and x_3 parallel to its edges (see Fig. 3.2a).

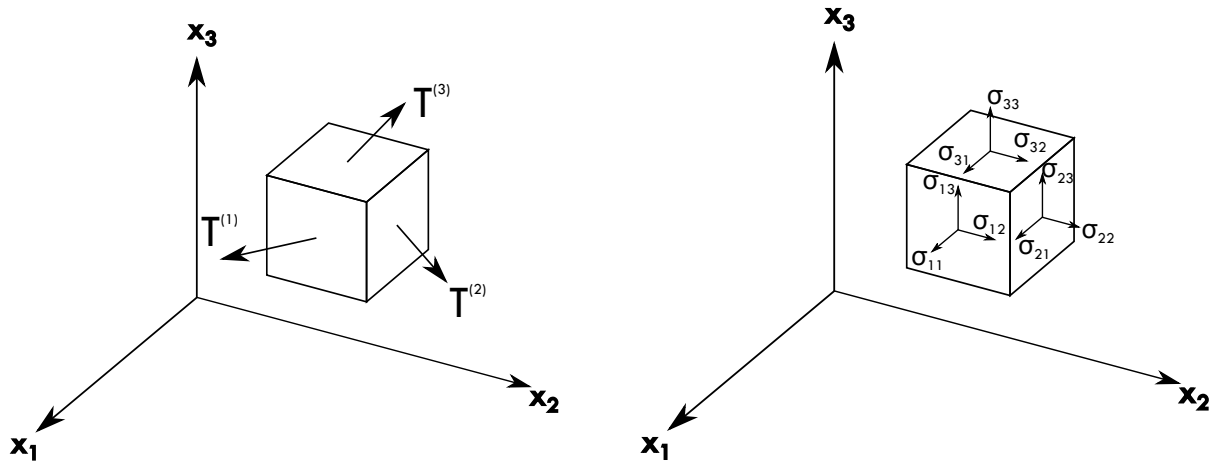

(a) An infinitesimal parallelepiped with traction vectors shown

(b) The nine forces acting on the parallelepiped

Figure 3.2: A body before and after deformation

The traction vectors $T^{(1)}$, $T^{(2)}$ and $T^{(3)}$ are shown and are referenced to the areas that they act upon by superscripting with the direction of the areas unit normal. Each of these traction vectors are made up of three Cartesian components; if $T^{(1)}$ is considered then it is composed of $T_1^{(1)}$, $T_2^{(1)}$ and $T_3^{(1)}$. These terms can be renamed using σ such that:

$$\begin{aligned} T_i^{(1)} &\equiv \sigma_{11}, \sigma_{12}, \sigma_{13} \\ T_i^{(2)} &\equiv \sigma_{21}, \sigma_{22}, \sigma_{23} \\ T_i^{(3)} &\equiv \sigma_{31}, \sigma_{32}, \sigma_{33} \end{aligned}$$

Or in a more compact manner:

$$T_j^{(i)} = \sigma_{ij}$$

The nine quantities comprising σ_{ij} are the stresses experienced at any given point within a body and the first subscript denotes the coordinate direction of the normal of the area the stress is acting on and the second subscript denotes the direction of the force intensity. These nine forces are shown in Fig. 3.2b. σ_{ij} can be described by an array:

$$\begin{bmatrix} \sigma_{11} & \sigma_{12} & \sigma_{13} \\ \sigma_{21} & \sigma_{22} & \sigma_{23} \\ \sigma_{31} & \sigma_{32} & \sigma_{33} \end{bmatrix}$$

The diagonal terms are known as the normal stresses as the force intensities coincide with the direction of the surface normal. The other terms are the shear stresses. The normal stresses can be either a tensile or compressive force; if tensile they point outwards from the interface and are assigned positive values, if compressive they vectors point inwards and are negative. The shear stresses are positive if both the intensity and the corresponding normal are both facing in a positive direction or both facing in a negative direction.

With further derivation, Cauchy's stress formula can be derived (Eq. 3.2.1). The derivation is out of the scope of this thesis but it is well documented in any mechanics of materials textbooks such as [Dym and Shames, 2013].

$$T_i^{(v)} = \sigma_{ij} v_j \tag{3.2.1}$$

Using Cauchy's stress formula above it is possible to relate any arbitrary traction vector with any direction to a set of nine stresses located at an orthogonal interface at any point in a body.

3.2.2 Strain

When the body is subjected to the stresses, it responds through deformation, a phenomenon that can be separated into two sub-categories: pure displacement (rigid body motion) and deformation (shape changes to the body). Deformation is described through the use of strains and the strain tensor.

When displacement occurs, the material remains entirely the same geometrically but the spatial position of points within the body will change; that is the body may move through a distance or rotate around a point. This means that a line segment between any two points within the body will remain at a constant length before and after loading. If any line segment changes length after the load application (there has been a change in the size or shape of the material) then the body has been deformed. To consider these changes, a body of arbitrary shape and volume will be considered (Fig. 3.3a) before and after deformation.

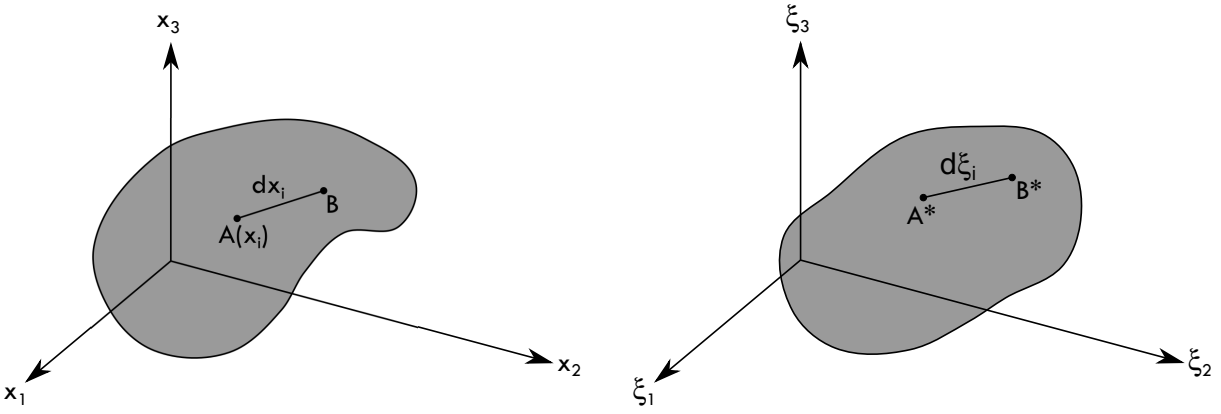

(a) A body before deformation occurs

(b) The same body after arbitrary deformation occurs

Figure 3.3: A body before and after deformation

Within the body, two arbitrary points A and B have been marked and located at positions x_i and dx_i respectively. A line segment has been drawn between them. As previously mentioned,

if a force is applied to the body, the change of length of any line segment can be used as a reference for the deformation of the body. From Fig. 3.3a the length of the line segment is determined as:

$$(\overline{AB})^2 = (ds)^2 = dx_i dx_i \tag{3.2.2}$$

When external loads are applied to the body, a deformation takes place and points A and B are moved to new points A^* and B^* as shown in Fig. 3.3b. It is worth noting that the x_i axis has been labelled the the ξ_i axis whilst analysing the deformed body. This occurs by mapping the each x_i coordinate to a ξ_i coordinate. Thus we can express the deformation as:

$$\xi_i = \xi_i(x_1, x_2, x_3) \tag{3.2.3}$$

A unique inverse to the above is also available due to the one-to-one mapping applied prior so that:

$$x_i = x_i(\xi_1, \xi_2, \xi_3) \tag{3.2.4}$$

Thus it is possible to express the differentials of dx_i and $d\xi_i$ by using the above relations:

$$\begin{aligned} dx_i &= \left(\frac{\partial x_i}{\partial \xi_j}\right) d\xi_j \\ d\xi_i &= \left(\frac{\partial \xi_i}{\partial x_j}\right) dx_j \end{aligned} \tag{3.2.5}$$

As a result an expression for the length of the original segment between points A and B, $(ds)^2$ (Eq. 3.2.2) can be found:

$$(ds)^2 = dx_i dx_i = \frac{\partial x_i}{\partial \xi_m}\frac{\partial x_i}{\partial \xi_k} d\xi_m d\xi_k \tag{3.2.6}$$

Likewise for the deformed state in Fig. 3.3b the line segment between point $\overline{A^*B^*}$ is found to be:

$$\begin{aligned} (\overline{A^*B^*})^2 = (ds^*)^2 &= d\xi_i d\xi_i \\ &= \frac{\partial \xi_i}{\partial x_k}\frac{\partial \xi_i}{\partial x_l} dx_k dx_l \end{aligned} \tag{3.2.7}$$

To investigate the deformation the change of length of the segment needs to be found. This can be done by either using Eqs. 3.2.6 or 3.2.8:

$$\begin{aligned} (ds^*)^2 - (ds)^2 &= \left(\frac{\partial \xi_k}{\partial x_i}\frac{\partial \xi_k}{\partial x_j} - \delta_{ij}\right) dx_i dx_j \\ (ds^*)^2 - (ds)^2 &= \left(\delta_{ij} - \frac{\partial x_k}{\partial \xi_i}\frac{\partial x_k}{\partial \xi_j}\right) d\xi_i d\xi_j \end{aligned} \tag{3.2.8}$$

These can now be re-written as:

$$(ds^*)^2 - (ds)^2 = 2\epsilon_{ij}dx_i dx_j \tag{3.2.9}$$
$$(ds^*)^2 - (ds)^2 = 2\eta_{ij}d\xi_i d\xi_j$$

Where ϵ and η are strain terms given by:

$$\epsilon_{ij} = \frac{1}{2}\left(\frac{\partial \xi_k}{\partial x_i}\frac{\partial \xi_k}{\partial x_j} - \delta_{ij}\right) \tag{3.2.10}$$

$$\eta_{ij} = \frac{1}{2}\left(\delta_{ij} - \frac{\partial x_k}{\partial \xi_i}\frac{\partial x_k}{\partial \xi_j}\right) \tag{3.2.11}$$

The first of these equations (Eq. 3.2.10) is the Green's strain tensor and is formulated in Lagrangian coordinates as it expressed in the undeformed state. The second equation is the Almansi Tensor and is a function of the coordinates of the deformed state. The rest of this section will merely be concerned with the Lagrangian form of the strains.

Up to this point, only the deformation of the body has been described by the Green strain formula in Eq. 3.2.10, however, it is necessary to observe the effects of displacement that could be in the form of rigid body motions. Here, the displacement field will be introduced as:

$$u_i = \xi_i - x_i \tag{3.2.12}$$

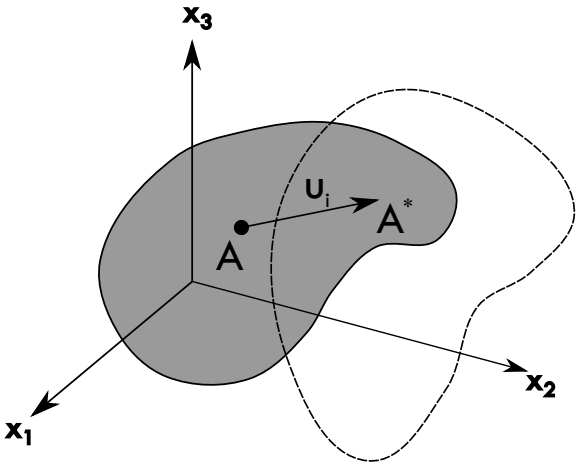

Figure 3.4: A body moved from a reference configuration to a deformed configuration

This u_i term expresses the displacement of every point in the body from the initial undeformed configuration and is shown in Fig. 3.4. The following relation can be developed from Eq. 3.2.12:

$$\frac{\partial x_i}{\partial \xi_j} = \delta_{ij} - \frac{\partial u_i}{\partial \xi_j} \tag{3.2.13}$$

Substituting the equation above into Eq. 3.2.10 the following is derived:

$$\epsilon_{ij} = \frac{1}{2}\left(\frac{\partial u_i}{\partial x_j} + \frac{\partial u_j}{\partial x_i} + \frac{\partial u_k}{\partial x_i}\frac{\partial u_k}{\partial x_j}\right) \tag{3.2.14}$$

This serves to show that strain is a second order tensor. Similarly to stress, strains can act in both normal and shear planes and are experienced at all points of a body. Now that the strains have been developed, a deformation function would be determined depending on the characteristics of the problem at hand. This will be discussed later in the thesis.

3.3 Mechanical Failure Criteria

Mechanical failure criteria are measures given to many different material classes. Failure criteria are available for both isotropic and anisotropic materials, however, a general requisite for a failure criterion is macroscopic homogeneity. In any case, a well-constructed failure criterion can discriminate between states of stress in a material that will lead to certain failure and states which are safe to use with a material.

'Failure' is a word that is commonly used in engineering yet isn't always easy to define. A general definition is that failure is reached when a material is no longer able to perform within its usual linear, reversible range of behaviour due to the effect of a major change to irreversibility. A general sense will be that the material can no longer support significant loads.

3.3.1 A Brief History of Mechanical Failure Criteria

The earliest failure criterion that has stood the test of time was developed by Coulomb in the 18^{th} century. It was applicable to isotropic materials subjected to three-dimensional (3D) stress conditions. The work was further improved and popularised by Mohr in the following century through the creation of Mohr's circle. The method developed a failure envelope for a given material; if the stress was within the plotted envelope then the material could withstand the stress without any loss of function; if the stress was outside of the plotted envelope then the material was predicted to fail [Christensen, 2017a].

As interest developed in material failure, von Mises was credited with perhaps the most used failure criterion for isotropic materials [Christensen, 2017b], which, is used to predict yielding in materials. In more recent times there has been a significant effort to develop failure criterion for anisotropic materials, particularly for fibre enforced lamina acted on by biaxial stresses. The World Wide Failure Exercise (WWFE) was launched in 1996 and concluded in 2004, a large exercise that ended with a 1200 page compendium. The exercise extensively tested nineteen popular theories, assessed their strengths and weaknesses and provided recommendations about which criteria would be most suitable for different applications.

Since the pioneering effort concluded in 2004, WWFE-II has taken place to develop criteria for crack propagation and material behaviour under triaxial stresses.

Ultimately, these exercises have demonstrated that even the most complex of theories has huge weaknesses and that application of such criteria requires a great knowledge of the problem at hand as well as an understanding of the selected criteria and its strengths and weaknesses.

3.3.2 How Would a Mechanical Failure Criterion for Living Human Tissue be Determined?

First of all, a classification of the material type will need to be determined. Like many dead materials, such as metals, tissue will have different characteristics depending on the viewing scale. When viewed within the cell wall, a cell is certainly inhomogeneous; the cytoplasm alone contains numerous elements of different mechanical properties and the nucleus has significantly different properties to that of the cytoplasm. However, at a macroscopic level, tissue behaviour could likely be described by a homogeneous model, an assumption that works well for many materials.

In the case of the cell, there are two primary 'materials'. These are the nucleus and the cytoplasm. However, if the cell is considered to be a homogeneous structure within the cell wall then certain approximations could be made. For example, when a sustained external force is applied to a cell, it causes the cell to deform as one body. It is assumed that cell tissue failure occurs when there is a failure to the either the cell membrane or the cytoskeleton. Whilst, the mechanism for failure is important, the key consideration is at what load can the cell be subjected to before recovery is no longer possible. If an answer can be found for this question then it would be possible to determine a mechanical failure criterion for a living tissue cell.

In this regard, a cell can be treated like any other material; at a certain point the cell is no longer recoverable.

Chapter 4

Gel Fabrication

A layer of alginate gel is applied on top of the cells before the compression experiment takes place. The gel has two purposes: firstly, as the cells are fully embedded and immobilised within the gel during the experiment the gel acts as a medium to transfer the stresses from the indenter to the cells, secondly, the gel is used as a reference for the strain states within the cells through comparison with the numerical model.

It is essential that the gel has certain mechanical characteristics in order to efficiently transfer the stresses to the cells as well as to be comparable to the numerical model.

The following section will introduce the gel fabrication methods as well as the characteristics of the gel itself.

4.1 Alginate Gel Definition and Use

Alginates are defined as a group of polysaccharides that are produced from a mixture of brown algae and bacteria [Gorin and Spencer, 1966][Govan et al., 1981][Rehm, 2009]. Alginates are widely used across many areas of production and biomechanics and they can have a wide variety of properties dependent on the type and parts of algae that they are cultivated from. Typically, alginates are used for their viscosifying properties for which they are used in the textile food and biotechnological industries [Donati and Paoletti, 2009].

For the purposes of this thesis, the viscous properties of alginate will be exploited to fabricate a gel which can be used for cell immobilisation. This is a common application of alginate gels in the biomedical field [Smidsrod and Skjaak-Brik, 1990].

4.2 Gel Fabrication

A key feature of alginate is that it is able to bind efficiently with divalent cations such as calcium ions, Ca^{2+}. This leads to the formulation of a hydrogel of which the mechanical properties can be changed through the change in chemical composition.

The gel is fabricated using a buffer solution, a calcium carbonate solution (to bind to the alginate to promote polymerisation) and D-glucono-δ-lactone (GDL) solution (used to release the calcium ions).

Brown algae sodium salt, calcium carbonate ($CaCO_3$) and GDL were from Sigma (St. Louis, MO). A Heppes Buffer Solution (HBS) was mixed so as to control the pH levels of the final

alginate gel. The HBS was composed of:

- NaCl - 145nM
- KCl - 5mM
- Heppes - 10mM
- NaOH (1M)- used to achieve a 7.5 pH

Calcium carbonate was mixed with HBS and sonicated for seven minutes at a 25% amplitude and a 0.5 cycle (Sonicator dr.hielscher UP 200s) to break the intermolecular interactions thereby increasing the overall surface area of the calcium source.

Alginate (1.5% w/v) was mixed with the sonicated calcium solution and agitated for 1hr. To ensure sterility the dispersion was then autoclaved (Buch & Holm Selecta) at 121°C for 30 mins. Once autoclaved, the mixture was chilled by surrounding the container with ice.

A fresh GDL solution was produced and mixed with the dispersion. This would release the calcium ions thus controlling the ionic cross-linking process. This new mixture was vortexed and immediately 2mm volumes were pipetted into ⌀35mm wells. This was undertaken within a sterile environment to ensure that the risk of contamination was minimised. The gel was set in an incubator at 37°C for at least 24 hours.

GDL was used to reduce the size of the calcium carbonate particles. This was important as smaller particle sizes reduced the surface area available to react with the alginate which increases the gel transition time [**?**]. The molar ratio of $CaCO_3$ (60mmol) to GDL was 0.5 to maintain a neutral pH. The GDL had to be freshly made to avoid full hydrolysation [Draget et al., 1989] which would result in an uncontrollable and inconsistent gelation; it is important to try and produce a homogeneous gel.

4.3 Gel Characteristics

During the experiment, the gel will be subjected to large deformation and as such will need to be described by a non-linear model. The gel maintains the ability to elastically return to its pre-deformed state, thus, it can be described by a hyperelastic model. This will make use of the finite deformation theory.

Unlike linear elasticity (where strains are sufficiently small that all governing equations can be linearised), hyperelasticity can account for non-linear material properties and large shape changes. Hyperelastic materials are able to sustain elastic straining through large displacement by storing strain energy (produced by the work done by the stress) as potential energy. This will be used to develop a deformation function to relate the stresses and strains within the gel. The deformation function can be used to extend the theory documented in Chapter 3.2.

Viscoelasticity is another non-linear behaviour for which deformation is comprised of two parts; an elastic component and a plastic component. Two terms are introduced to describe the elastic and viscous components for a viscoelastic solid; the stored modulus and the loss modulus. The stored modulus represents the elastic portion and the loss modulus represents the dissipated

energy. In some cases the viscoelastic solid can be described using an elastic model, however, this is only possible if the loss modulus is small in comparison to the storage modulus.
The gel used in this experiment is characterised by a combined hyperelastic and viscoelastic model. The model was derived and is documented in the work by [Rasmussen, 2013]

Chapter 5

Numerical Investigation

A numerical model will be used in the future to determine and visualise the strains that are induced within the alginate gel during the compression experiment. The visualised strain state will be used as a reference for the strain state that is induced within the gel, and by association, the cells, during the experiment.
Whilst the model will serve no purpose in this project, it an essential component for achieving the project aim and as such will be documented here for a complete understanding of this work.

5.1 Finite Element Analysis

Finite Element (FE) method is a branch of mechanics which is used in all areas of engineering. The core theory behind FE is discretisation, the idea that any body, structure or space can be broken down from a continuous medium into a mesh comprised of numerous sub-areas/ -volumes called elements. Governing polynomial interpolation functions can thus be evaluated in a piecewise fashion across the entire body or structure. The method is extremely versatile as it can be used to calculate many different quantities (such as stresses, strains, magnetic flux, thermal flow and fluid flow) and can be used on complex geometries for which other analysis methods would struggle.

An FE model was created for this project by previous Aalborg University alumni and is well documented in [Rasmussen, 2013]. The FE process and configuration will be documented here for clarity.

In this experiment, a layer of alginate gel is used to cover the cells. The stiffness of the gel is orders of magnitude greater than the stiffness of the cells and it can be assumed that this results in the cells following the deformation of the gel. The purpose of the FE model is to investigate the strain distribution of the gel and by association, to investigate the induced strains within the cells. The strains calculated across the underside of the gel are of the most interest as these will be the strains experienced by the cells.

The gel is modelled in ANSYS Mechanical APDL, 14.0 (ANSYS, Inc.) and is discretised into a mesh consisting of plane, two-dimensional (2D) elements. Elements are connected together into a mesh at nodal points, which, ensures continuity of the displacement field and enables an equation field to be formulated for the entire geometry of the gel. Each node in the geometry is associated with a finite number of degrees of freedom (DOF). The elements are described by polynomial interpolation functions and each element evaluates the solution by sums. Boundary conditions are imposed to best model the experiment and to restrict unwanted motion and rigid body motions.

ANSYS will be used to calculate the strains in the gel. Of most interest, the shear strains, γ, will be investigated. These are of most interest due to possibly uninvestigated results obtained by [Breuls et al., 2003] that suggested cell death was sensitive to shear straining. The maximum shear strains, γ_{max} will be calculated throughout the entire gel with those found along the bottom surface of the gel being of most interest. In ANSYS, the maximum shear strains are defined as:

$$\gamma_{max} = \epsilon_1 - \epsilon_3 \tag{5.1.1}$$

Where ϵ denotes the principal strains.

To reduce complexity, reducing both modelling, manipulation and simulation times, symmetry can be imposed to reduce the model to a 2D axisymmetric model. This is possible due to the fact that the loading and boundary conditions are symmetrical.
As for the experiment, as described in Chapter 6, the indenter is displacement driven. The cells require straining of between 20% and 50%, this is considered to be large strains which means that a non-linear analysis will need to be undertaken. It renders the use of infinitesimal strain theory inadequate. As a result, the finite deformation theory will need to be applied and geometric non-linearities will occur due to non-linear strain-displacement relations. The geometric non-linearities can be considered to be large displacement, large strain and probably large rotation.

In addition to the non-linear material properties, viscoelastic properties will need to be built into the model as this best suits the properties of the gel.
Finally, there are additional geometric non-linearities that arise from the contact between the indenter and the gel; the contact area is unknown and is a non-linear function of displacement.

In summary, the model is comprised of geometric, material and geometric contact non-linearities.

5.2 Methods

This section will briefly introduce the settings and configuration used for the FE model as created by [Rasmussen, 2013].

The gel was modelled using a mesh of plane, 4-node elements (PLANE182) with axisymmetric element options turned on. This enabled the three-dimensional (3D) model to be reduced to a 2D model. The material parameters for the model were based on the tensile tests documented in [Rasmussen, 2013]. Elements were formulated using reduced integration with hourglass control to reduce the effects of shear and volumetric locking that can occur with these elements.

Solution accuracy was verified by assessing the ratio of artificial energy (AENE) to total energy (SENE). Any ratio of less than 5% is typically an acceptable result.

The 2D model was modelled in the xy-plane so as to take advantage of the axisymmetric capabilities in ANSYS. The y-axis was used as the axis of symmetry and the x-axis was aligned

in the radial direction along the upper surface of the gel.

To model the interaction between the indenter and the top surface of the gel, contact elements were required. The aluminium indenter was modelled using the target elements (TARGE169). In the experiment, the indenter is orders of magnitude stiffer than the gel and is considered to be undeformable. In ANSYS it was modelled as a rigid body which removes any internal forces or stiffness calculations meaning that it is computationally inexpensive in comparison to a mesh of deformable elements. The indenter was modelled using a pilot node with six DOF and was only able to translate in the y-axis during simulation. The upper surface of the gel, already meshed with antisymmetric elements, was overlaid with the contact elements (CONTA172).

The contact algorithm used for the simulation was the Augmented Lagrange algorithm. Typically it provides the best surface to surface contact, minimises penetration and is less sensitive to the magnitude of the contact stiffness in comparison to other contact algorithms.

For element contact detection points, Gauss integration points were used. These are specially selected points within the element which provide the most accurate results.

Contact problems are complex and there are many formulation variables that need to be controlled. Steps were taken to eliminate gaps and interferences and this would also ensure that unwanted rigid body motions were avoided.
Due to the large strains, non-linearity was selected for the model. The generalised form of the Maxwell model was used to model viscoelasticity. The relaxation function was represented by a Prony series.

5.3 Discussion

In future experiments, the numerical model will be a major component for developing a mechanical failure criterion for living human tissue. This will be the only tool used as a measure for the strains within the gel and by association will determine the strain state with the cells themselves.

The material model for the gel was verified by comparing the tensile performance of a gel sample to that of a gel patch modelled in ANSYS. This simple test demonstrated a good correlation between the properties of the modelled gel and the real gel.

The material parameters for the gel were obtained from a tensile test of the gel, however, during the experiment, the gel is going to be subjected to compressive loading. It is likely that when the gel is compressed it will exhibit different response behaviour when compared to tensile loading. In the future, it may be necessary to design and perform a compressive test on the gel to investigate whether there is any change in the material properties or behaviour. These parameters could then be used to update the FE model and would ensure that the model is as accurate as it could be.

Chapter 6

Experimental Procedure

An experiment has been developed to investigate the large-scale effects of strain state on the rate of change of cell viability. This chapter will introduce the experiment as a whole as well as documenting and discussing the results that are obtained when the experiment is performed.

6.1 Materials and Equipment

The section below will list all of the materials and equipment used during the mechanical experiment.

6.1.1 Cells

To model muscle tissue, the C2C12 cell line will be used. These cells are myoblast cells that are capable of propagating into muscle fibres after differentiation.

The C2C12 cells originated in 1977 through the serial passage of myoblast cells obtained from the thigh muscle of C3H mice.

6.1.2 Cell Culture and Staining

C2C12 murine skeletal muscle myoblasts (passages 15-30) were expanded in 75cm^2 flasks. The growth medium is composed by DMEM, 4.5g/L Glucose w/ L-Glutamine, 10% fetal calf serum - FCS (Gibco, cat. no: 10270-106), 1% penicillin 10 U/ml / Streptomycin 10 mg/ml (Invitrogen, cat. no: 15140-122), 0.5% Gentamycin 10mg/ml (Invitrogen, cat. no: 15710-072).

Cell passage was perfromed when cells reached about 70% confluence to avoid premature differentiation. Cells were plated on 35mm plates with an initial density of 1×10^5 cells/cm^2 and left in the incubator (35°, 5% $C0_2$)for 24 hours.

Staining Method 1

The cells are stained with a mixture of propidium iodide(PI) and calcein. The cells are washed with HBS before having a staining solution applied. The cells are then incubated (35°, 5% $C0_2$) for one hour before being washed once more by HBS to remove excess calcein. Finally, a fresh PI solution is applied to the cells (in the same concentration as before but without the addition of calcein).

PI is used as an indicator for cell death. When it bonds with nucleic acid it emits a strong red fluorescence when excited by a green light source. The PI can only bond to the nucleic acid through permeation of the nucleus membrane which suggests significant cell damage.

Calcein is used to indicate living cells by providing a green fluorescence when excited by a blue light. Once the cells have been presented with calcein for an hour, they should be washed with HBS as a prolonged calcein presence begins to make the cells cloudy which inhibits the microscopic image evaluation.

Staining Method 2

Cells are pre-tagged with a green fluorescent protein (GFP) expression. This eliminates the need for calcein staining. PI staining is achieved as before.

This method was only used for the fourth (final) cell experiment but should have no bearing on the cell viability.

6.1.3 Gel

A layer of alginate gel will be used to cover the cells during the experiment. The purpose of the gel is to immobilise the cells and to transfer stresses to the cells when the indenter is applied.

The fabrication method and characterisation of the gel are documented in Chapter 4.

6.1.4 Mechanical Test Set-Up

The experiment will be conducted using an Olympus IX70 inverted microscope with 10x magnification. The microscope includes a motorised bi-translation platform (Prior).

A Zeiss AxioCam MRm r3 camera is used to capture images. This camera is only capable of capturing black and white images.

An indenter system has been constructed so that it is attached to and moves with the microscope platform. The indenter is controlled by a manually driven hydraulic controller capable of displacing a minimum step of 2μm. The indenter is custom made with a rounded tip and is attached to a pressure sensor (Sauter FH-5 digital force gauge).

6.1.5 Experimental Control

The experiment is semi-automatically controlled. A control programme is used to automatically control the motorised platform, create all necessary files and instruct the user at all points of the experiment. The user is required to manually focus the microscope when required, manually capture images, alternate light filters (between blue and green illumination) and control the shutter.

The experimental control programme is an in-house computer programme created in Python3 (Anaconda).

Micro-Manager 1.4 was used to observe live images through the camera and was used to capture images.

6.2 Experimental Methods

A compressive time-lapse experiment has been developed to investigate the effects of strain on the rate of change of cell viability as shown in Fig.6.1. The investigation requires a sequence of microscopic images to be captured over a wide area of a cell sample. The image sequence will be repeatedly captured numerous times at regular time intervals. Comparison of the obtained images will show the deterioration of the cells with respect to time. By comparing the deterioration rates of loaded cell samples to control samples it will be possible to determine the effects of mechanical loading.

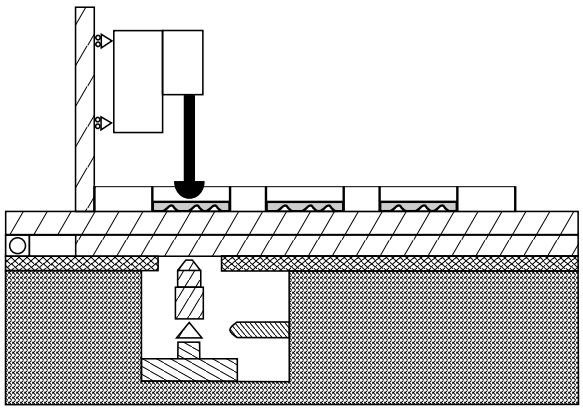

Figure 6.1: The experimental test set-up

The pre-stained cells (see Section 6.1.2) are contained within a multi-well plate which has the capacity to hold six individual cell samples. In each experiment, only three wells will be used; two cell samples will be covered with alginate gel (Chapter 4) and the third will be left uncovered. This enables an investigation into the effects of the applied load with control samples to negate the effects of both the gel and the test environment.

The multi-well plate is placed on the microscope platform, positioned above the inverted microscope. A compressive load is applied to the very centre of the first cell well (Well 1) through the use of a custom made indenter with a rounded tip which induces a variable strain state within the cells.

The indenter is lowered using a manual, hydraulically controlled displacement driver until it makes contact with the top of the gel layer (contact is indicated through the use of a pressure sensor and the position is noted as being at height 'zero'. The indenter is then forced into the gel and into the cells. It is a displacement controlled experiment. The experiment is now initiated and the cells in Well 1 will undergo sustained loading until the experiment is concluded. The focus of the rest of this section will be entirely on the loaded cells in Well 1.

When the indenter is forced into the gel a variable strain state is induced within both the gel and the cells which cause the cells to begin to die. The induced strain field extends beyond

the field of view of the microscope and as such, a sequence of images is required to capture the full effect of the indenter. Due to the symmetric effects described in Chapter 5, the strain field should be the same along any radial path taken from the centre of the cell well and directed outwards.

This investigation aims to establish whether mechanical loading has an impact on cell viability, and whether a variable strain field changes the rate of change of cell viability.
In future, the strain state at all points within the cell well will already be known from the numerical investigation (Chapter 5), by referencing it to the FE model. It will, therefore, be possible to investigate the effects of strain state on cell viability by observing how many cells are dead or dying within different regions of the strain field. The number of dead or dying cells is also known due to cell staining techniques as described above in section 6.1.

To record the effects of the induced strain state, a sequence of images is captured starting at the centre of the well and moving radially outwards in a known coordinate plane. The process is achieved by capturing an image before moving the cells through a small displacement relative to the microscope. This process is repeated until a panoramic-style sequence of images is obtained. The image sequence needs to be captured twice for every time-step; the first image sequence is captured with blue light illumination and the second image sequence is captured with the green light illumination (to capture living (green) and dead cell (red) fluorescence respectively). These two image sequences represent one step in the time-lapse experiment; the same image sequences will be re-captured after waiting for an allotted time period. This is undertaken for all three wells.

Through observation of an image sequence for any individual time-step, it will be possible to see the distribution of dead cells relative to the application point of the load. Through comparison of the image sequences obtained for a current time-step, to that obtained by the previous time-step it will be possible to investigate the rate of change of cell viability.

A quantifiable study could be obtained by referencing the strain state within the cell well to that obtained by FE model.

6.3 Analysis: Image Processing and Procedure

The experiment obtains data in the form of image sequences captured over several time steps. Analysis of the data is required to investigate; the cell viability distribution for each time step in every cell sample, the effects of strain state on cell viability for the loaded cells and the rate of change of cell viability for all cell samples. Several processes have been considered so as to determine the most suitable analysis methods regarding ease of use, accuracy and repeatability.

To illustrate the different analysis methods that have been considered, the first step of the first experiment will be used as an example. Experiment 1 was a three-well experiment and for each time-step, each well required six images per sequence (twelve images in total accounting for both the green and red channels). The experiment was composed of seven time-steps meaning that in total 252 images were captured and needed processing.

Fig. 6.2 shows a typical data set obtained for a single time-step for a given well. First, the image sequence was captured for the green channel (6.3a), then the platform returned to the

initial position and the same cells were captured for the red channel (6.3b). These images are captured in monochrome but can be merged together using ImageJ to create a coloured composite image (6.2c). The information obtained from these images will be discussed in the

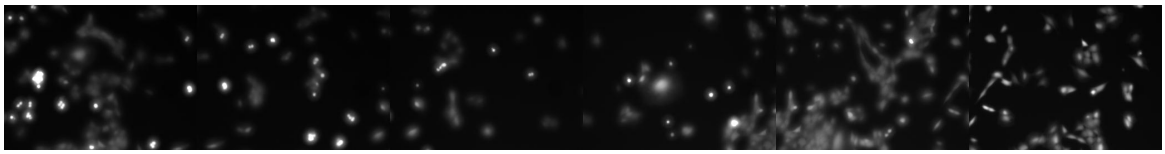

(a) Green channel

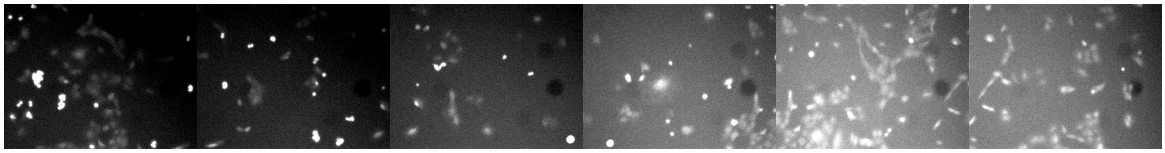

(b) Red channel

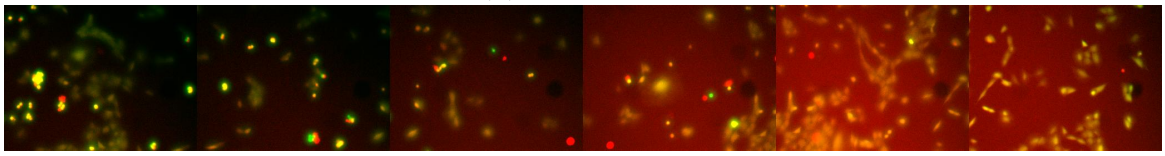

(c) Green and red merged composite image (merged using ImageJ(Fiji))

Figure 6.2: Typical data set for a single time step for a given well

following sections, here, the focus will be on the different processing methods that have been attempted and various procedures that have been considered.

6.3.1 Image Stitching

The images shown in Fig. 6.2 are individual images positioned side by side with one another. It is possible to see that there is an overlap between any two sequential images in the series, where, cells are captured twice in neighbouring images. This was specifically programmed into the platform control software so as to allow for image stitching possibilities, as demonstrated in Fig. 6.3. The advantage of image stitching lies in the fact that it can be certain that there is no missing data between images whilst ensuring that each cell is only accounted for once in the final stitched image. This increases the speed and accuracy of analyses such as cell counting.

The images in Fig. 6.3 were stitched together using the ImageJ stitching plugin [Preibisch et al., 2009] and whilst the images included here have been well combined, the process took a long time to complete due to the fact that the images had to be stitched together in a pairwise fashion. To create these two panoramic images, it took a combined time of approximately one hour, as each subsequent image in the sequence was individually added to a steadily increasing panoramic of its predecessors. Regions of interest (ROI) were manually implemented to speed up the process but the method was impractical and would require a period of days or longer to have performed stitching for all images. Moreover, in some instances stitching wouldn't be possible; the process requires that each pair of neighbouring images in a sequence share recognisable features, which, isn't always the case.

The stitching plugin does include functions for bulk image stitching, however, for the images obtained in this experiment the functions either failed to work, took too long to process or had poor results. Bulk image stitching would also allow for colour composite images to be stitched

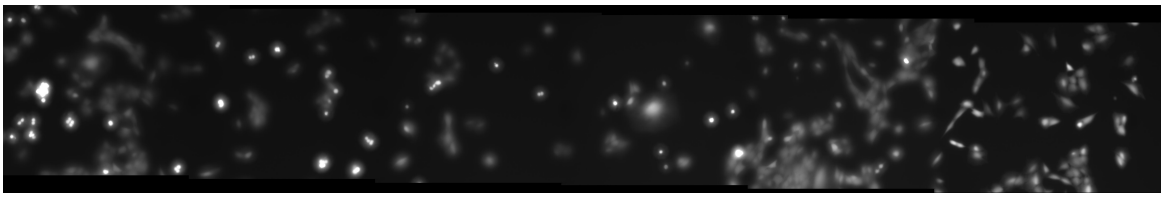

(a) Green channel

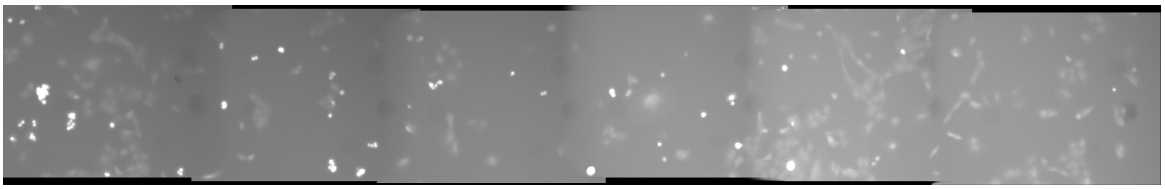

(b) Red channel

Figure 6.3: Experiment 1; Indented; t=0: example of stitched images using Image J stitching plugin

together directly, a more difficult task when stitching in a pairwise fashion. It is possible that these functions could be made to work but unfortunately, time constraints stopped the development of this feature and the additional benefits of image stitching were outweighed by the negatives of producing the images.

Despite this, image stitching for cell experiments has been widely used and the ImageJ stitching plugin has been implemented extremely successfully for many cell applications. It is likely that this could be implemented for this experiment in the future.

6.3.2 Automatic Cell counting

ImageJ includes functions for automatic cell counting and originally it was thought that these functions could be used to provide a quantitative image analysis of all of the images obtained over four experiments.

As an example the very first image shown in Fig. 6.3a will be used to demonstrate the automatic cell counting process in ImageJ.

Fig. 6.4 shows the key processing steps for automatic cell counting. Some steps have been omitted such as: applying basic brightness and contrast enhancements to the original, out of camera image; reducing the image from 16-bit to 8-bit; and, converting the image to a mask.

The process is cumbersome and takes time; it is necessary to go through the ImageJ file system frequently and each step adds processing time. The accuracy of the final count is also questionable. Fig. 6.4e shows the outlined cells and the cell count (each cell is numbered internally although it is too small to perceive this in this printed image.) It is quite apparent that by comparing this image to the out of camera image in Fig. 6.4a that the automatically obtained dead cell count is somewhat short of the real number. The final image count was totalled at 17 dead cells but it is easy to count more than that by eye.

The issue occurs during the thresholding process. This can be seen through the comparison of Figs. 6.4b and 6.4c where some of the clearly defined cells within a cell cluster in the former

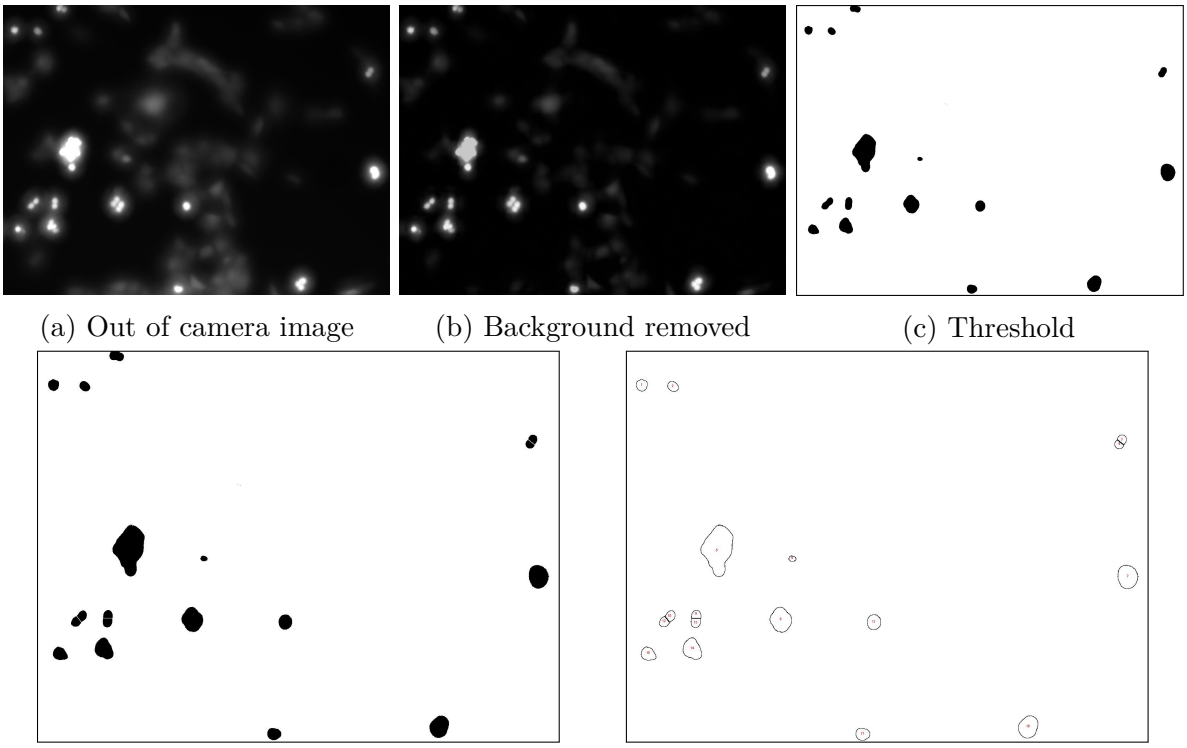

(a) Out of camera image (b) Background removed (c) Threshold

(d) Watershed (e) Cell counting

Figure 6.4: Experiment 1; Indented; t=0; Image 1: cell counting using ImageJ

image are grouped together into one body and counted as one cell in the latter. The threshold could be increased so that some of the lower intensities in the cell cluster would be removed. This would increase the definition of cells within the cluster, however, this would likely result in some of the other cells being removed from the final image.

To deal with this problem, the watershed algorithm (applied in Fig. 6.4d) is used to detect and divide cell clusters in the thresholded image. It has successfully divided some of the conjoined cells, but it too is limited and has failed to separate some obvious clusters. In other images, the watershed algorithm over-divides so that the automatically obtained cell count is significantly higher that the real count.

A macro was created to speed up the cell counting process but produced poor results due to the thresholding process being difficult to automate consistently.

These methods could be revisited but it would require more consistent images to be captured straight from the camera itself.

6.3.3 Final Analysis Process

Despite the technology available to us, a manual method is still deemed the most suitable method for investigating the cell viability. It is believed that an automatic analysis method is achievable in the near future but this will be discussed in Chapter 7.

6.4 Results

This section will document the results obtained from the cell experiments. Four experiments were undertaken and every result will be presented here grouped by experiment. Each experiment will have the results presented by well; Well 1 will always be the gel covered loaded cells, Well 2 will be the cells covered with a layer of alginate gel and Well 3 will be the natural cells.

6.4.1 Cell Experiment 1

This experiment was the initial experiment undertaken. Each time-step required six image positions per well. Seven time-steps were taken and occurred at time: t=0, t=1hr, t=2hrs, t=3hrs, t=20hrs, t=22hrs and t=24hrs.

Experiment 1: Well 1 (Loaded Cells)

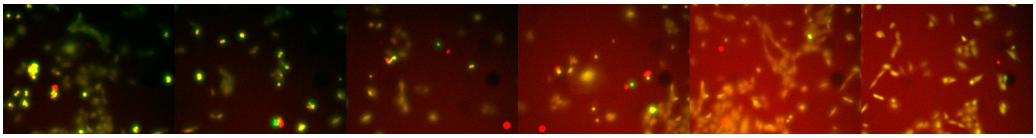

(a) Step 1: t=0

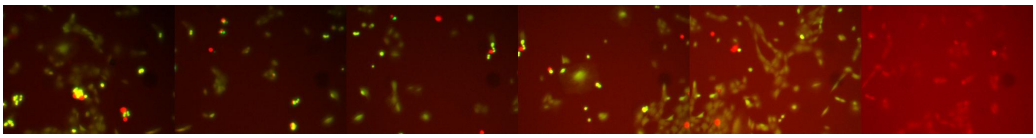

(b) Step 2: t=1hr

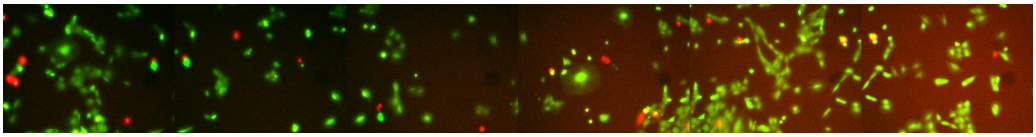

(c) Step 3: t=2hrs

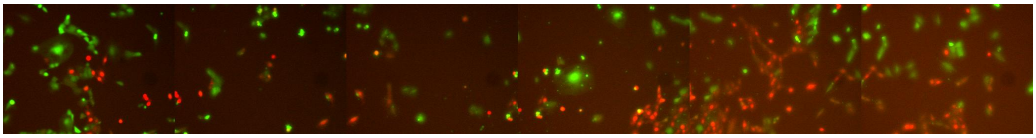

(d) Step 4: t=3hrs

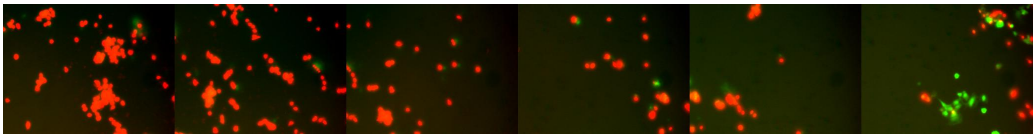

(e) Step 5: t=20

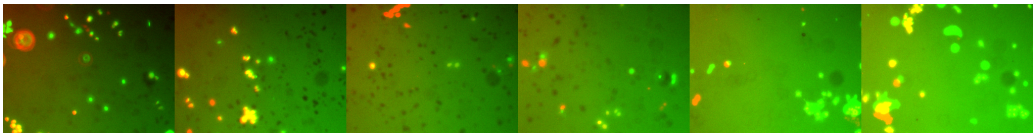

(f) Step 6: t=22

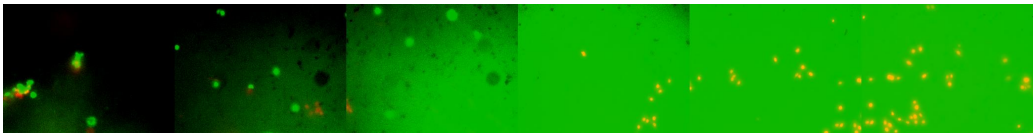

(g) Step 7: t=24

Figure 6.5: Experiment 1; indented cells

Well 1 Results Summary

Taking the first time-step in the series, it is apparent that there are dead cells immediately within the sample (these are the brightest cells; either a bright, strong yellow or a very defined red colour). The majority of the dead cells are contained within the first four images of the sequence, those closest to the centre point of the indenter. After one hour some changes seem to occur (Fig: 6.5b): firstly, there has been some definite cell movement (in the first image as the bright cell cluster of dead cells has moved and translated a considerable distance); secondly, there is an increase in cell viability in the fifth image in the sequence.

The cell viability seems to remain fairly consistent until the fourth step of the time lapse when there was a significant change in the numbers of dead cells (the bright red cells in the images). The number of dead cells increased across the entire image sequence (comparing Figs. 6.5d and 6.5c), however, the most significant increase occurred within the last three images of the sequence, towards the edge of the indenter area.

Unfortunately, this experiment was quite short and the next images were captured twenty hours after the experiment was initiated. At this point, almost all of the cells had died and the process that led to the cell death was untracked.

Interestingly, the final three images provided some experimental insight which could be used for the remaining experiments. In Figs. 6.5e, 6.5f and 6.5g there is a lack of intermediate tonality; that is that the image is almost entirely red or green and there is very little in between. This was due to calcein clouding the cells; prior to this experiment it was not known that the calcein should be washed from the cells after an hour of incubation. This meant that finding focus in the images was particularly difficult and the overall image quality was poor.

Experiment 1: Well 2 (Gel Covered Cells)

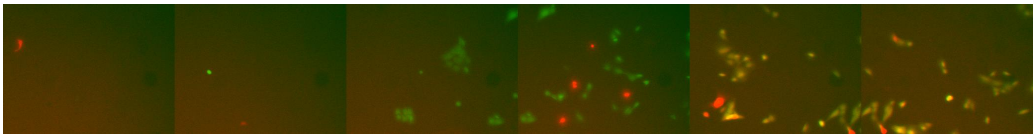

(a) Step 1: t=0

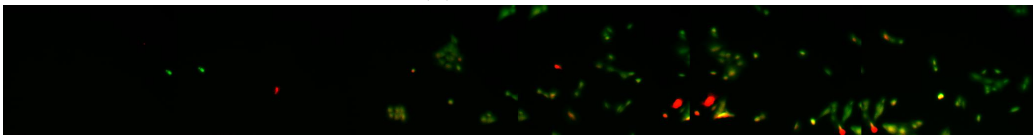

(b) Step 2: t=1hr

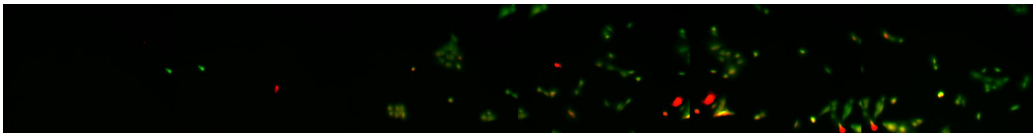

(c) Step 3: t=2hrs

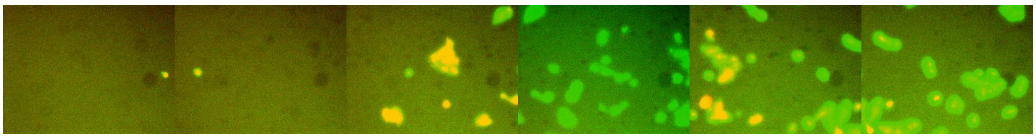

(d) Step 4: t=3hrs

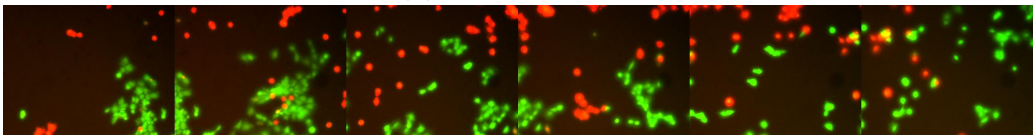

(e) Step 5: t=20hrs

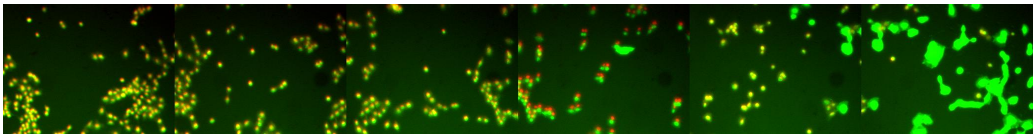

(f) Step 6: t=22hrs

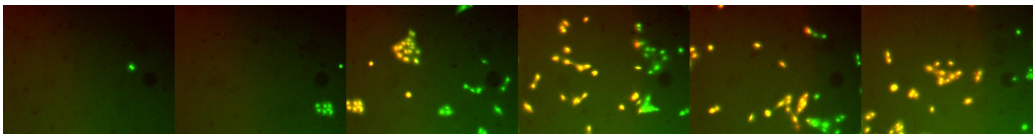

(g) Step 7: t=24hrs

Figure 6.6: Experiment 1; gel covered cells

Well 2 Results Summary

This well suffered from cell sparsity. For example, the first two images obtained for the first time-step (shown in Fig. 6.6a) have one small cell in each. These cells were also difficult to locate and to focus on as they were quite dim (a problem exacerbated by the exposure problems).

Three hours after the experiment was initiated, there is still no change in the cell viability of the image, a significant difference to the behaviour exhibited in the loaded cells.

In steps 5 and 6 (Figs. 6.6e and 6.6f) a completely new set of cells appears to be shown. It would have been possible perhaps that after seventeen hours some cells had moved although this doesn't seem to be the case due to the fact that in the image sequence for step 7 the original cells are once again shown. One possible explanation for this is that there was a floating layer of dead cells that happened to be there at this point. This could be supported by the fact that all of the cells have shifted a significant distance in the two hours that occurred between steps 5 and 6 and also in the fact that red and green channels in step 5 don't match up. Alternatively, it could have been a software error in the platform control programme but it is unusual that it returned to the same location in step 7.

One final possibility is that the cells were in another focus plane. This had been noticed in other experiments and could have been made possible by the low exposure settings. Take the first image from the initial time-step (Fig. 6.6a): the overall image is quite dull and underexposed with one red cell. It is possible that the only light detectable on the noisy, monochrome live image was that red cell and as such this was the focus plane that was set for the experiment. Twenty hours later, when returning to the experiment, it becomes apparent that there are many more cells in another plane and naturally these are the cells that are selected for imaging.

Regardless of whatever happened, step 7 shows that even after twenty-four hours, all of the cells have died. It may appear that there are still some cells living, however, this was caused by some small illumination problem where the green light filter was not properly lined up with the laser. This meant that it didn't quite cover the whole of the frame. This can be confirmed by looking at the right-hand side of an image and comparing it to the left-hand side of the neighbouring image. For example the second and third images in the sequence shown in Fig. 6.6g: in the second image the cluster seems to be living but in the third image it becomes apparent that it is fluorescent in the red channel.

Experiment 1: Well 3 (Natural Cells)

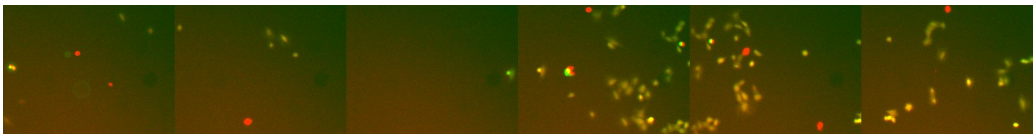

(a) Step 1: t=0

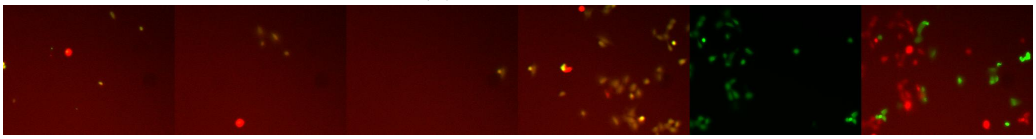

(b) Step 2: t=1hr

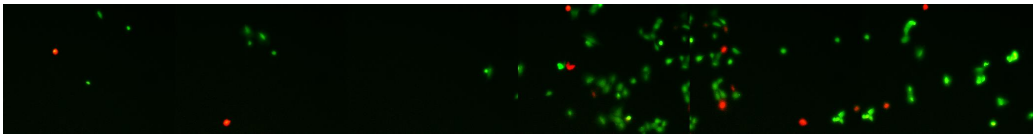

(c) Step 3: t=2hrs

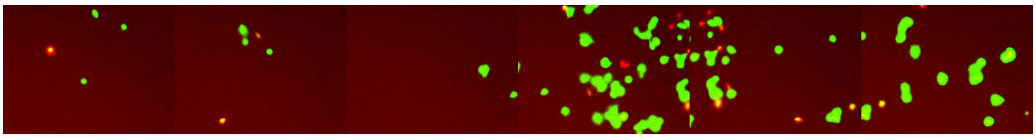

(d) Step 4: t=3hrs

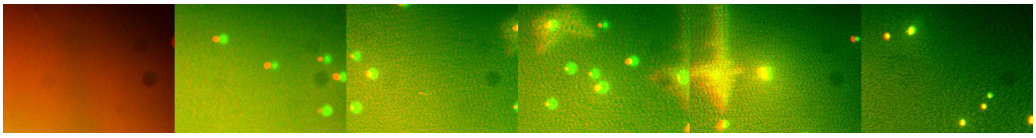

(e) Step 5: t=20hrs

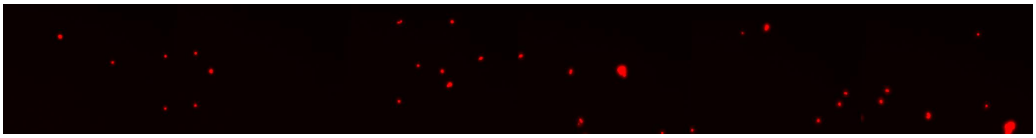

(f) Step 6: t=22hrs

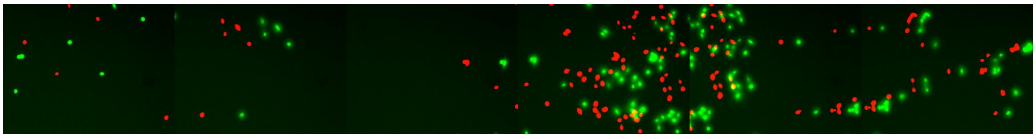

(g) Step 7: t=24hrs

Figure 6.7: Experiment 1; natural cells

Well 3 Results Summary

Well 3 is similar to Well 2. There are many spots with limited numbers of cells and the images are fairly similar. There are low numbers of dead cells throughout the first three hours of observation and after twenty hours all the cells are dead. The image sequence in step 5 appears to capture the gel rather than the cells but this was likely due to some focusing issues.

6.4.2 Cell Experiment 2

This experiment was a repeat of the previous experiment, however, this time there would be ten images obtained per sequence and there would be eleven time-steps taken at times: t=0, t=1hr, t=2hrs, t=3hrs, t=4hrs, t=5hrs, t=6hrs, t=7hrs, t=8hrs, t=20hrs and t=24hrs.

Well 1 (Loaded Cells)

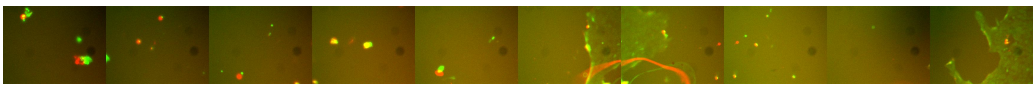

(a) Step 1: t=0

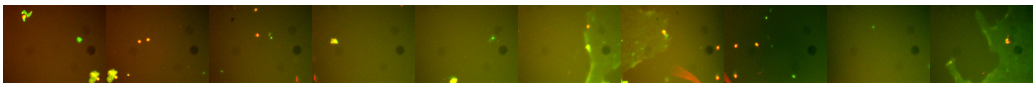

(b) Step 1: t=1hr

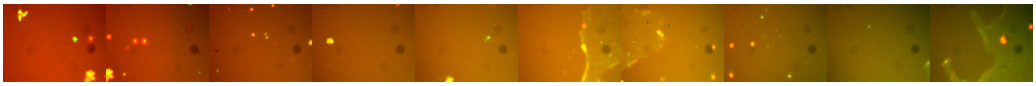

(c) Step 4: t=3hrs

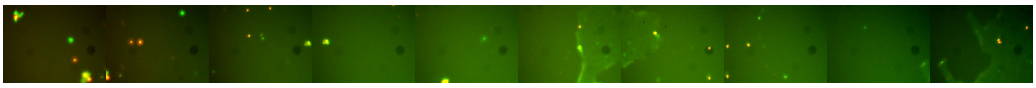

(d) Step 5: t=4hrs

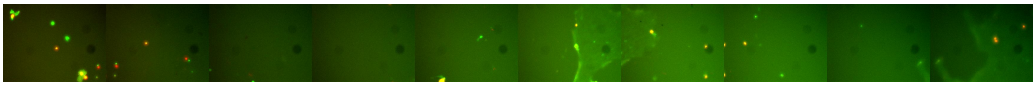

(e) Step 6: t=5hrs

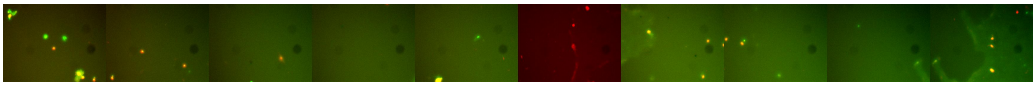

(f) Step 7: t=6hrs

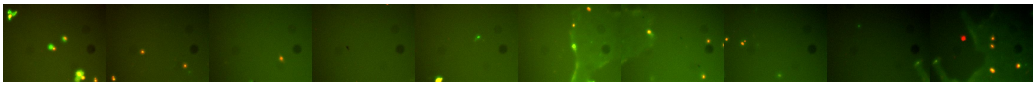

(g) Step 8: t=7hrs

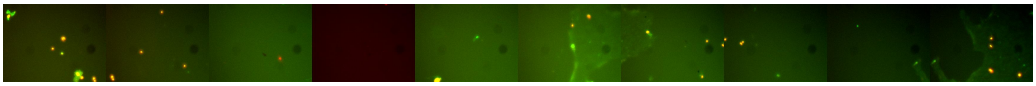

(h) Step 9: t=8hrs

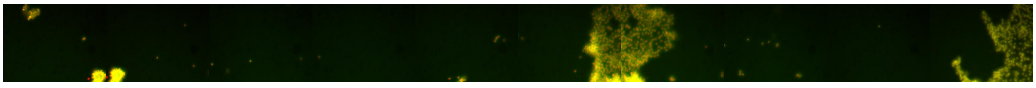

(i) Step 10: t=20hrs

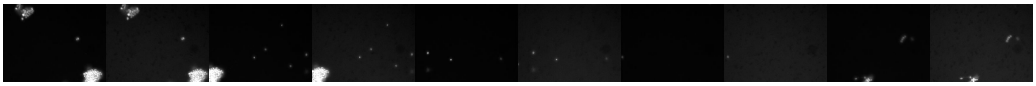

(j) Step 11: t=24hrs

Figure 6.8: Experiment 2; indented cells

Well 1 Results Summary

Overall this experiment suffered from cell sparsity issues.

Initially in the first time-step (Fig. 6.8a) obtained at time t=0 it is clear that of the few observed cells, the cell viability is low: almost all of the cells within the first five images of the sequence are dead. In the sixth image, it appears that there is a large group of cells that have split from the sample. There are dead cells at all points in the sequence.

After an hour of testing there appear to be some additional dead cells, particularly in the seventh image of the sequence (Fig. 6.8b). There has also been some cell movement detected, in the fourth image the cell clusters have drifted to the left.

There are no significant changes until step 9 (8 hours of loading). It now appears that all the cells have died within the first five images of the sequence (Fig.6.8h).

After twenty hours it appears that all of the cells are dead; the two large cell clusters are clearly made of thousands of cells and all of these have died overnight (Fig. 6.9j).

In the final image ((Fig. 6.8j), a problem occurred with the image capturing and the platform didn't move to the expected positions. The image is monochrome as it was only captured with the red channel.

Well 2 (Gel Covered Cells)

Well 2 Results Summary

The sample suffered from cell sparsity, which, hampers analysis as there are fewer cells to comment on.

In the initial image captured at time t=0 (Fig. 6.9a), there appears to be one dead cell in the entire sequence (appearing twice, once in the fourth and once in the fifth images in the sequence). The sixth image of the sequence seems to be captured only with the red channel, this was due to an experimental error.

The image sequence is shown in Fig. 6.9e suffered from exposure issues, which, limited the post-processing possibilities and led to the strangely coloured image.

Throughout the first eight hours, there is little to no change although it appears that there are some dying cells as they are a weak yellow colour.

Finally, after twenty hours, all cells seem to have died. Additionally, there are cells that weren't previously visible found in the latter three images.

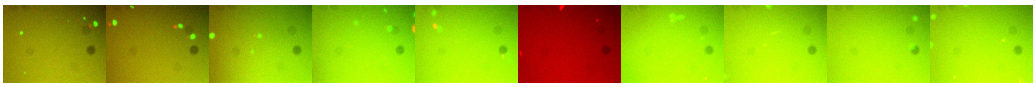

(a) Step 1: t=0

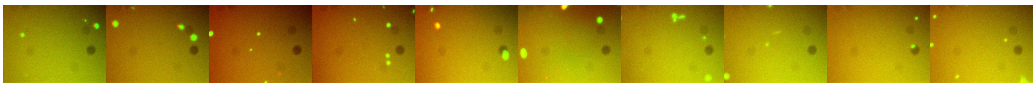

(b) Step 2: t=1hr

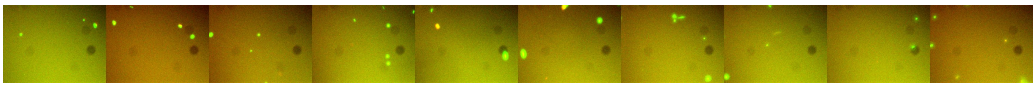

(c) Step 3: t=2hrs

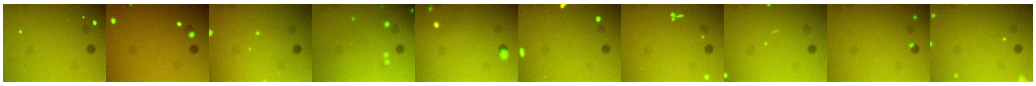

(d) Step 4: t=3hrs

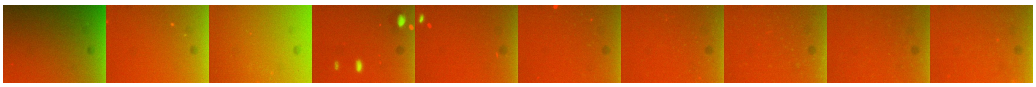

(e) Step 5: t=4hrs

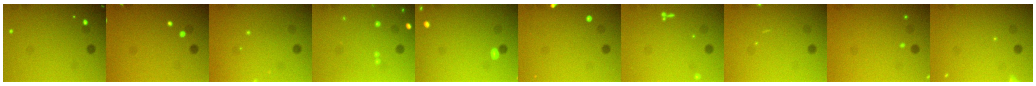

(f) Step 6: t=5hrs

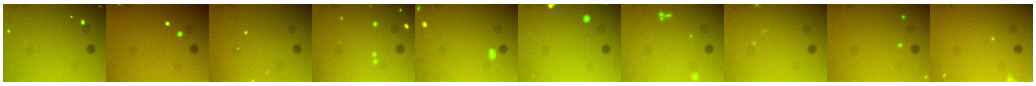

(g) Step 7: t=6hrs

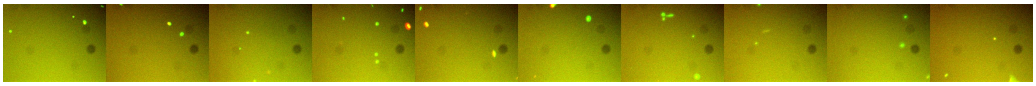

(h) Step 8: t=7hrs

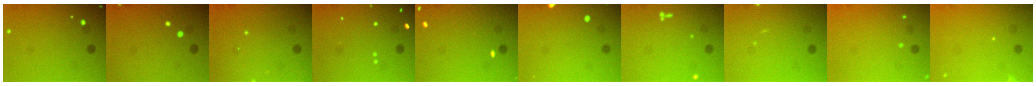

(i) Step 9: t=8hrs

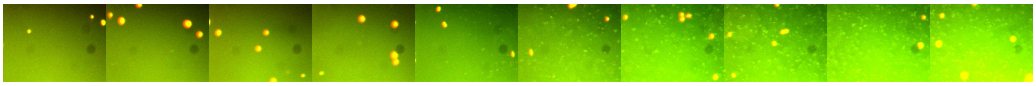

(j) Step 10: t=22hrs

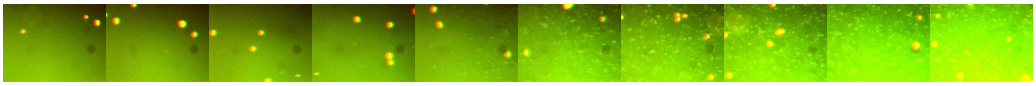

(k) Step 11: t=24hrs

Figure 6.9: Experiment 2; gel covered cells

Well 3 (Natural Cells)

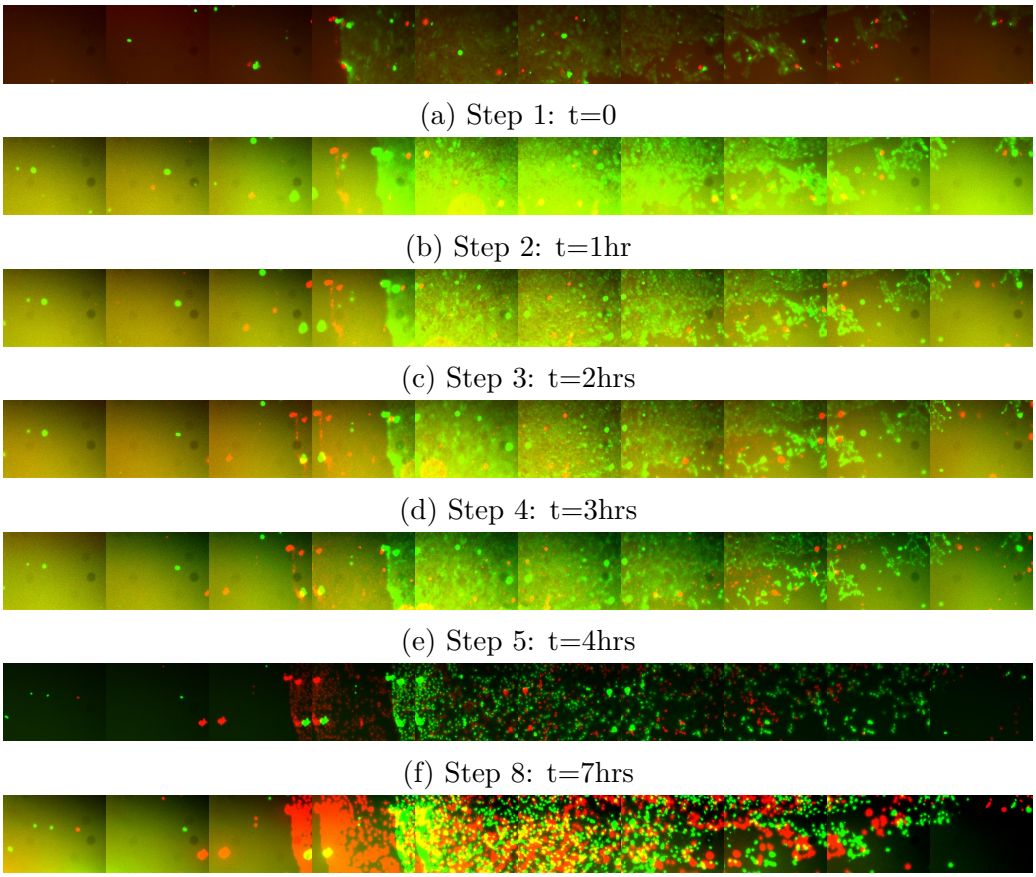

(a) Step 1: t=0

(b) Step 2: t=1hr

(c) Step 3: t=2hrs

(d) Step 4: t=3hrs

(e) Step 5: t=4hrs

(f) Step 8: t=7hrs

(g) Step 9: t=20hrs

Figure 6.10: Experiment 2; natural cells

Well 3 Results Summary

Immediately it is apparent that there is less data than for the other two wells. This was due to file corruption issues (a problem that can occasionally occur in ImageJ when saving images as stack files).

This sample has most of the cells contained within the middle of the image sequence. At time t=0, there is a high cell viability, with very few dead cells relative to the overall number of visible living cells.

Figs. 6.10b to 6.10b suffered from exposure problems when capturing the images which meant that it was difficult to merge the images. Looking at the fifth image of each of the sequences at the bottom edge there is a big, bright, yellow circle. This is due to the exposure issues as it appeared so much brighter than the rest of the image. Correctly judging the exposure prior to capture could have resolved this.

Gradually as this experiment progressed, the images obtained for the red channel and those obtained for the green channel became more and more unsynchronised. In Fig. 6.10a the red and green channels are well aligned, however, in Fig. 6.10g the red channel is shifted to the

left by almost a full image. This must have been a result of a platform control error but this will be described later.

After seven hours of testing, there are in fact many dead cells (Fig. 6.10f) The majority of these are found on the boundary of the cell sample, where there is a densely populated 'ridge' of cells.

After twenty hours, all of the cells are dead in the sample.

6.4.3 Cell Experiment 3

This experiment was a repeat of the previous experiment, however, this time there would be ten images obtained per sequence and there would be ten time-steps taken at times: t=0, t=1hr, t=2hrs, t=3hrs, t=4hrs, t=5hrs, t=6hrs, t=7hrs, t=22hrs and t=24hrs.

Well 1 (Loaded Cells)

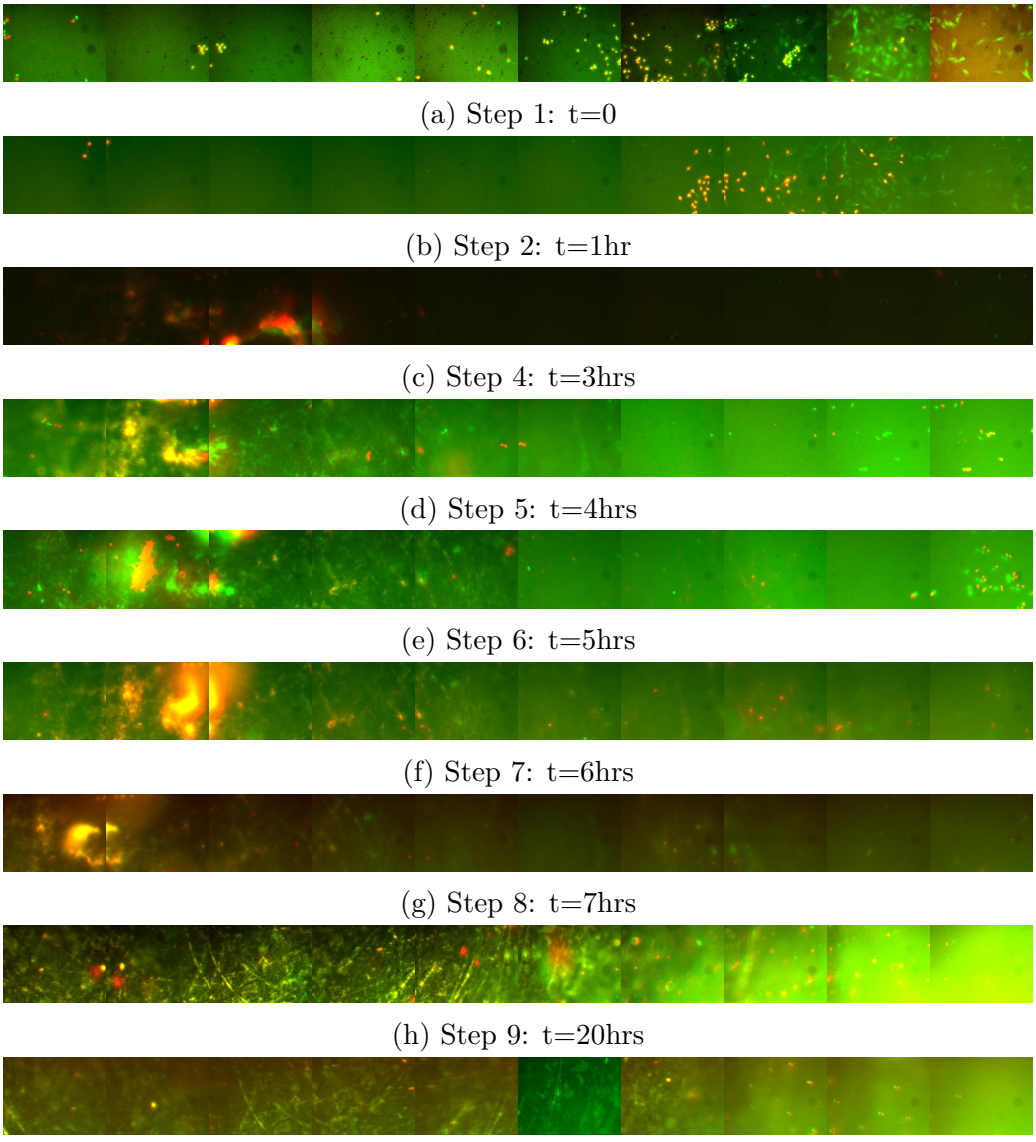

(a) Step 1: t=0

(b) Step 2: t=1hr

(c) Step 4: t=3hrs

(d) Step 5: t=4hrs

(e) Step 6: t=5hrs

(f) Step 7: t=6hrs

(g) Step 8: t=7hrs

(h) Step 9: t=20hrs

(i) Step 10: t=24hrs

Figure 6.11: Experiment 3; indented cells

Well 1 Results Summary

When looking at all of the obtained image sequences shown in Fig. 6.11, it is immediately apparent that there are a lot of discontinuities on display. These problems were caused by focusing issues that were exacerbated by poor exposure settings.

Initially, when the indenter is applied, there are immediately a lot of dead cells throughout the sequence (Fig. 6.11a). There are few cells within the first five images of the sequence but the overall percentage of cell death is higher than for the later images in the sequence which are furthest from the maximum impact point of the indenter.

After an hour of loading, all cells seemed to have died in the sample, although the cells observed seem to be different. This could be because of a platform control problem, some moving cells or focus issues. Focusing issues will be discussed later in this chapter.

From steps 2 to 8 a strange phenomenon occurs, where, this fluorescent cloud seems to be floating in the cells. This could have been because of an incident when the microscope lens pressed into the cell well plate pushing, it upwards and pressing the indenter into the base of the plate, effectively crushing the gel and the cells beneath it. The incident happened when trying to observe another well. This could perhaps have crushed numerous cells releasing the nucleic acids which would then bond with the applied PI stain.

Looking closely at the third to fifth images within the image sequences shown in Figs. 6.11e and 6.11f it is possible to see part of the indenter. It is unclear whether this is the centre of the indenter or not; if it is it implies that the indenter has moved relative to its initial position.

The results for this well were not as expected or desired. Too many issues crept into the results, however, what is clear is that there seemed to be an effect from the indenter on the viability of the cells. This is demonstrated by the fact that all of the cells appeared to have died within an hour of loading.

Well 2 (Gel Covered Cells)

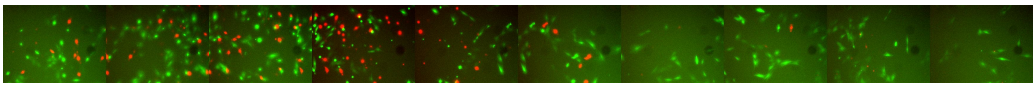

(a) Step 1: t=0

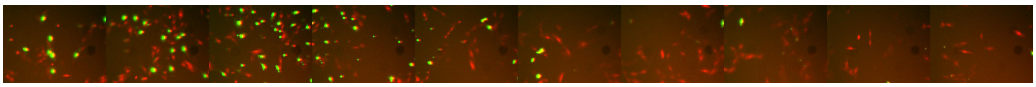

(b) Step 2: t=1hr

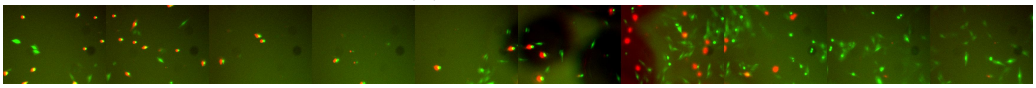

(c) Step 3: t=2hrs

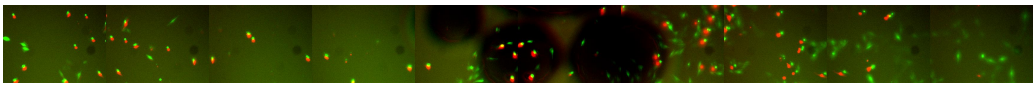

(d) Step 4: t=3hrs

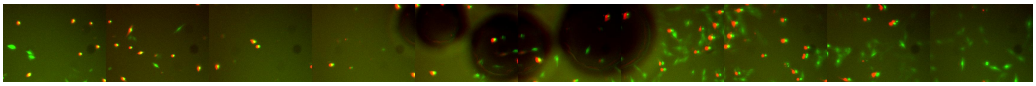

(e) Step 5: t=4hrs

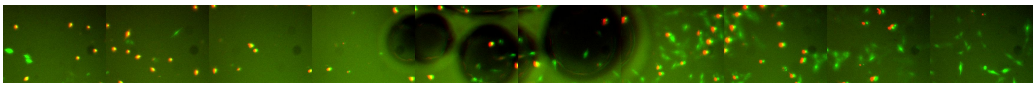

(f) Step 6: t=5hrs

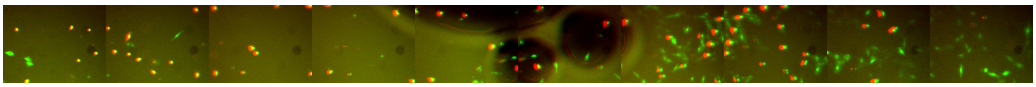

(g) Step 7: t=6hrs

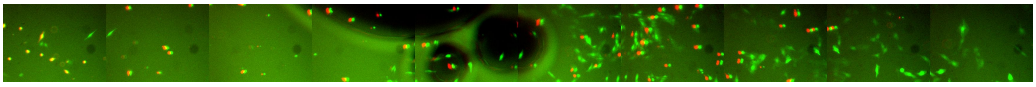

(h) Step 8: t=7hrs

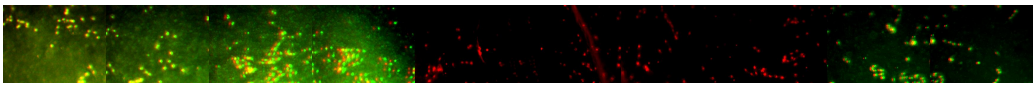

(i) Step 10: t=22hrs

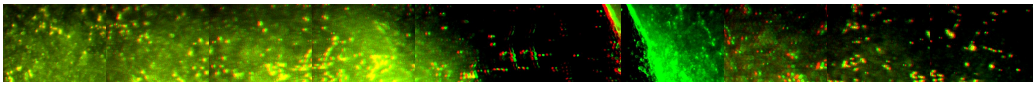

(j) Step 11: t=24hrs

Figure 6.12: Experiment 3; gel covered cells

Well 2 Results Summary

Initially there are a fair amount of dead cells present within the sample with the majority found within the first six images of the sequence (Fig. 6.12a). There seems to be little change in cell viability the following hour (although the images appear to have been merged incorrectly (the red channel should be the green channel and visa-versa).

Over the next seven hours, the cell viability remain more or less consistent although the cells seem to be moving slowly to the left. From the third step in the time lapse some bubbles seem

to come into the frame; these were trapped under the alginate gel when it was applied. Despite this, there seems to be little to no change in the cell viability numbers throughout the duration of the experiment until time t=22hrs when all cells had died.

Well 3 (Natural Cells)

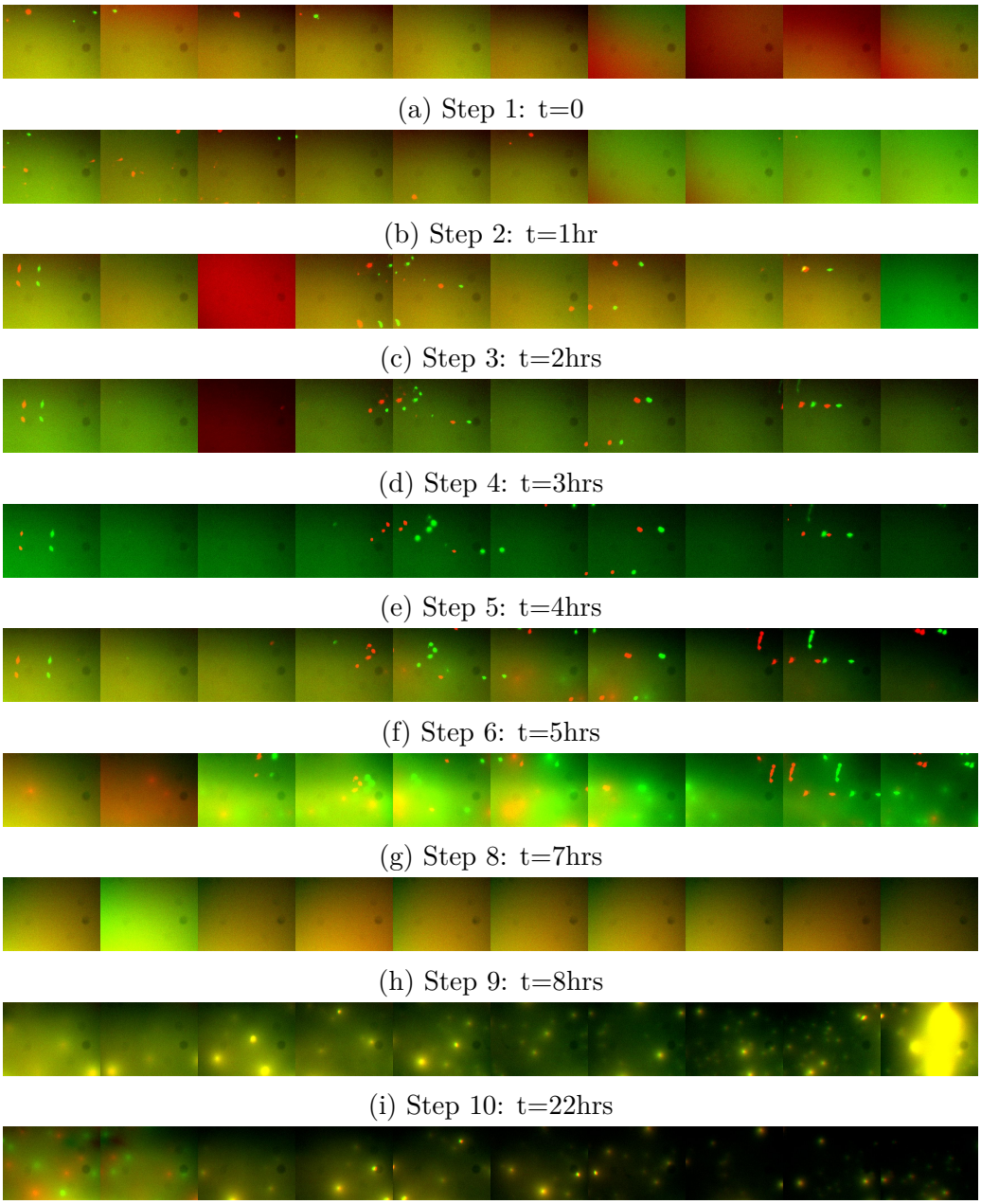

(a) Step 1: t=0

(b) Step 2: t=1hr

(c) Step 3: t=2hrs

(d) Step 4: t=3hrs

(e) Step 5: t=4hrs

(f) Step 6: t=5hrs

(g) Step 8: t=7hrs

(h) Step 9: t=8hrs

(i) Step 10: t=22hrs

(j) Step 1: t=24hrs

Figure 6.13: Experiment 3; natural cells

Well 3 Results Summary

This cell sample had relatively few cells in the observed region and those that existed appeared to have died from the very beginning of the experiment.

As the experiments continued in to step 3, some more cells started coming into view. This was because of focusing problems, where the cells captured in the first image were in a completely different plane to the cells captured in the fourth image of the sequence onwards. The dead cell count was of a high percentage throughout. In step 6 there is some apparent clouding of

the cells. The reason for this is unclear.

Overall the images obtained for this well (and the experiment as a whole) were somewhat disappointing.

6.4.4 Cell Experiment 4

Experiment 4 was expected to be a 24-hour experiment, however, due to a mechanical breakdown with the microscope platform, the experiment was reduced to a six-hour experiment with seven time-steps for Wells 1 and 2 but only a five-hour experiment with six time steps for Well 3. Time-steps were obtained at times: t=0, t=1hr, t=2hrs, t=3hrs, t=4hrs, t=5hrs and t=6hrs* (for Wells 1 and 2).

Experiment 4: Well 1 (Loaded Cells)

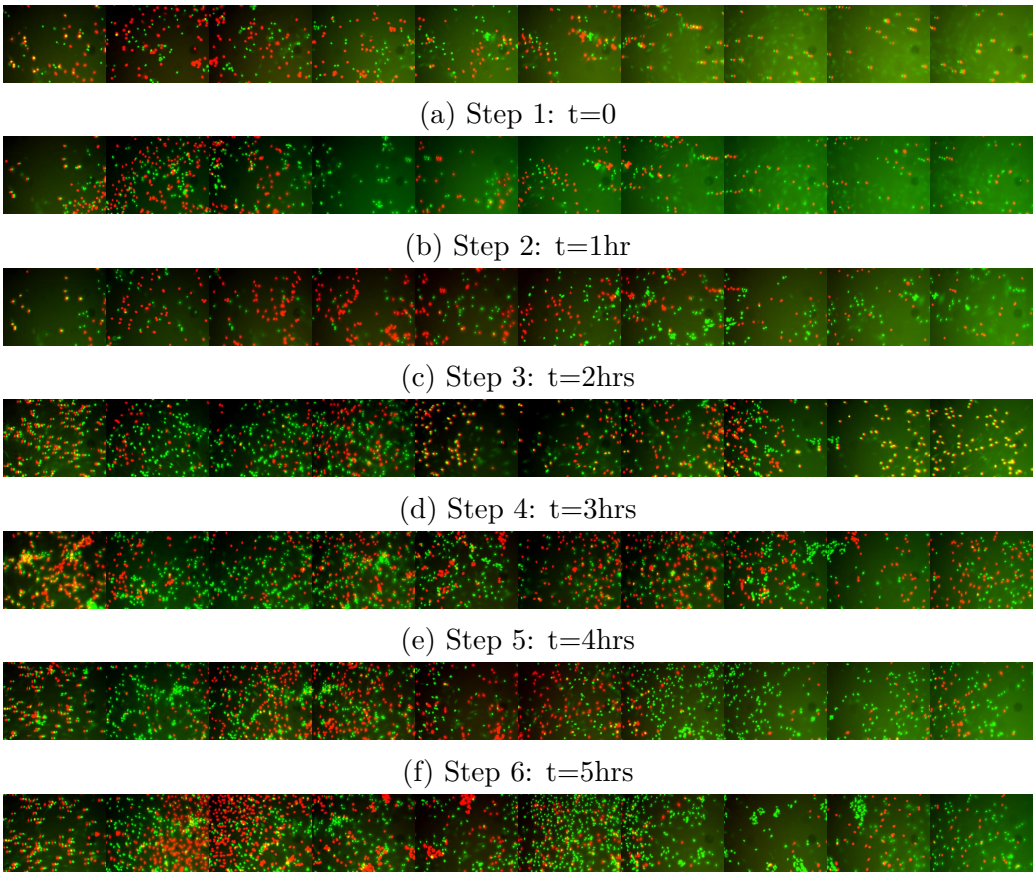

(a) Step 1: t=0

(b) Step 2: t=1hr

(c) Step 3: t=2hrs

(d) Step 4: t=3hrs

(e) Step 5: t=4hrs

(f) Step 6: t=5hrs

(g) Step 7: t=6hrs

Figure 6.14: Experiment 4; indented cells

Well 1 Results Summary

Looking at the images for Well 1 (Fig. 6.14) the initial images in steps 1 (6.14a) and 2 (6.14b) show that there are a high percentage of dead cells across the full sequence almost immediately. Between these steps, the cell viability remains fairly consistent but with an increase in

the number of dead cells in the second image of the second step. In Fig. 6.14b the fourth image is missing the red channel, a mistake when obtaining the data.

Two hours into the experiment and the cell viability has changed significantly (Fig. 6.14c). The changes are predominantly in the middling images (fifth - seventh images in the sequence).

Unfortunately, at the initiation point of step 4, some mechanical errors started to creep into the experiment; the motor stopped working at this point and the experiment had to be reset. This delayed the experiment by one or two minutes but the major problem was that the framed cells were now different to those that were initially being observed. Fig. 6.14d shows the images obtained for step 4. Although the cells in these images are not identical to those previously, the two sets were local to each other (likely within a millimetre) and the current cells were still directly under the indenter. This is to say that the new cell sample was still representative of the old sample and the results shouldn't instantly be dismissed.

During the third and fourth hours of testing the cell death numbers slowly increased across the full sample. The two channels don't line up perfectly for all images, which, can make the data harder to interpret but the clarity of the images shows a significant increase in the percentage of red cells across the range.

The final two hours of observation recorded a significant rise in the number of dead cells in the second and third images of the sequence. The first image appears to have a 100% dead cell rate and there are increases throughout the first half of the sequence. A similar pattern was observed as for all of the preceding images; a higher percentage of dead cells are observed in the areas closer to the centre of the indenter and there is a gradual decrease towards the furthest recorded point. Despite this decrease, there are sustained high numbers of dead cells noted across the full image sequence.

Overall it appears that over the six hours of testing there was a definite increase in the numbers of dead cells in the sample. Initially, there was a high percentage of dead cells particularly at the centre of the well, directly under the indenter. Over the next three hours, the cell viability steadily increased with a higher rate of cell death occurring through the middle of the sequence. This had the effect of having a more even cell viability distribution from images 1-7 in the sequence. In the last recorded hour of testing there seemed to be a large increase in the number of dead cells directly under the indenter area. In summary, it appears that the cell viability increased in the sample as the distance from the centre of the cell well (and indenter) increased.

Experiment 4: Well 2 (Gel Covered Cells)

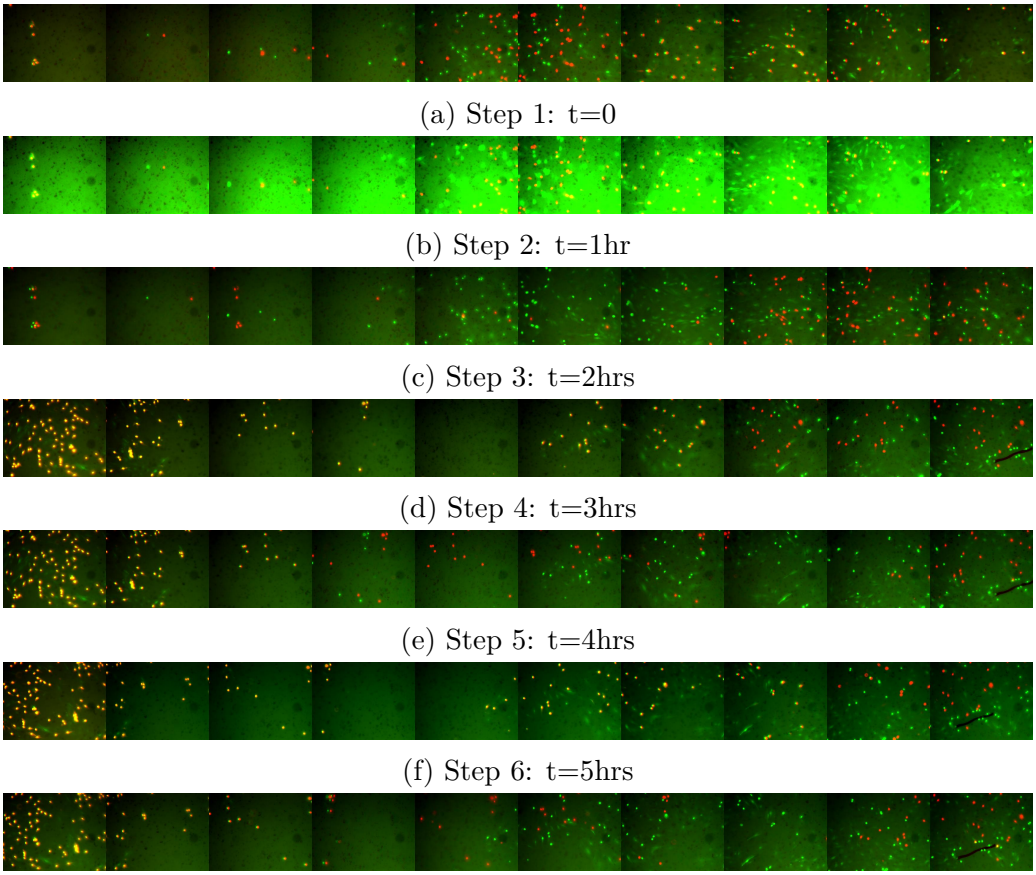

(a) Step 1: t=0

(b) Step 2: t=1hr

(c) Step 3: t=2hrs

(d) Step 4: t=3hrs

(e) Step 5: t=4hrs

(f) Step 6: t=5hrs

(g) Step 7: t=6hrs

Figure 6.15: Experiment 4; gel covered cells

Well 2 Results Summary

In Well 2 there were a significant number of dead cells as soon as the experiment commenced, however, the distribution of the dead cells was quite different from that of Well 1 and the overall number was significantly less than that of the loaded cells. In Fig. (6.15a) it appears that there are a higher proportion of dead cells situated in images 5-9 of the image sequence. Whilst there appear to be many dead cells in the 5th and 6th images of the sequence, the overall count appears to be less than that obtained for the corresponding images from Well 1.

After two hours there seems to be little change in the cell viability across the whole sequence. In the third hour, as previously stated, the experiment had to be restarted. The first two images of the new sequence (Fig. 6.15d) have a high proportion of dead cells (similar to the corresponding images obtained for Well 1). Unlike Well 1, however, the cell viability remains almost constant throughout the next four hours.

Experiment 4: Well 3 (Natural Cells)

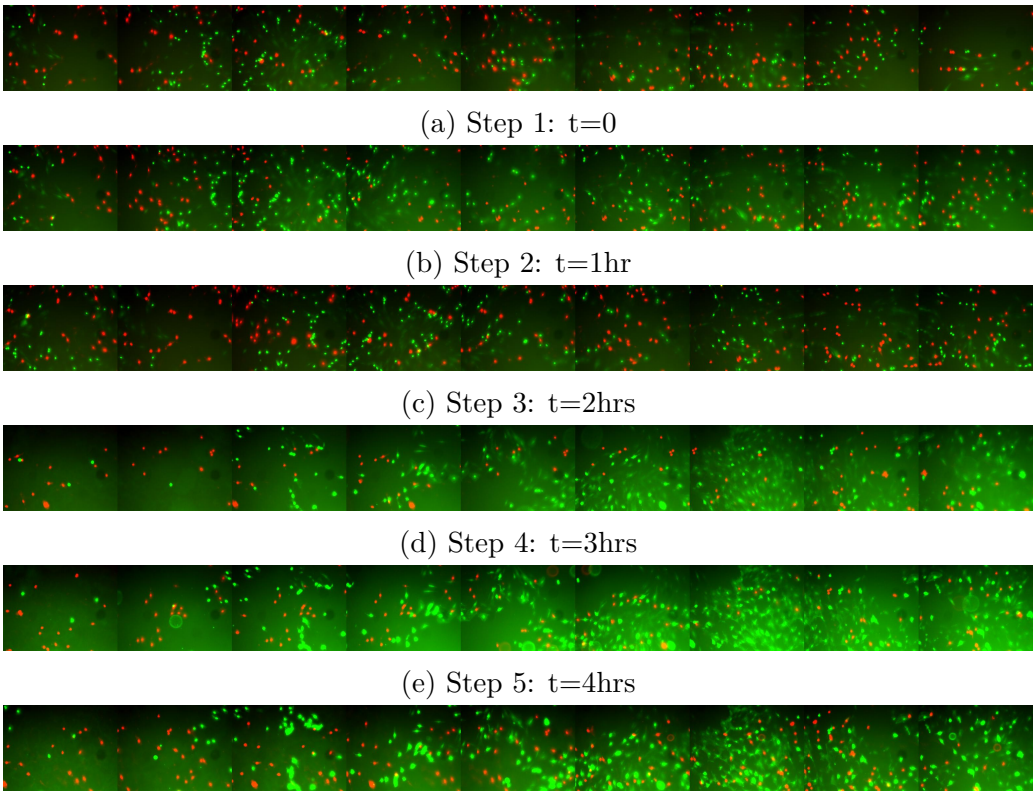

(a) Step 1: t=0

(b) Step 2: t=1hr

(c) Step 3: t=2hrs

(d) Step 4: t=3hrs

(e) Step 5: t=4hrs

(f) Step 6: t=5hrs

Figure 6.16: Experiment 4; natural cells

Well 3 Results Summary

Finally, Well 3 and the natural cells will be discussed. The was a high number of dead cells immediately in the well, albeit, less than the number of dead cells observed in the loaded sample. The overall distribution of the dead cells was fairly consistent across the whole image sequence. As the test continued the cell viability remained fairly consistent with little to no change observed across the entire five hours of testing.

6.5 Discussion

Overall the experiments provided some useful information but were let down by some experimental errors. Experiments 1-3 were particularly poor in terms of the data obtained. This was due to a lack of understanding of how best to control the exposure when capturing the images with Micro-Manager 1.4. There were other problems that arose in the first three experiments and much was learned during the experimental process.
Experiment 4 was expected to be the experiment where everything went right but it was affected by an unforeseen mechanical breakdown which ended the experiment prematurely. The problem was caused by one of the microscope platform's stepper motor drive screws coming loose from the motor, which thus rendered the control programme useless. Before running this

experiment, much care was taken to eliminating each problem that had occurred during the previous experiments:

- Exposure issues were solved by measuring exposures for both channels and making use of a live histogram to ensure even images were captured
- The indenter issues were solved by using both the live camera images and the computerised display for the pressure sensor to ensure that contact was made with the top surface of the gel.
- The problem of the microscope lens making contact with the platform or the cell plate was fixed by controlling the focal distance that could be achieved by the focus wheel.
- The cells used had already been tagged using GFP (see Section 6.1.2) which meant that they already displayed green fluorescence without the need for additional staining. This was useful because it meant that the cells could be looked at pre-experiment to determine that there were sufficient cell numbers in the areas of interest within the cell wells and this eliminated cell sparsity issues

Overall, the final processed images obtained by Experiment 4 are of a much greater quality than those obtained from the previous three experiments. This is primarily due to implementing the the live histogram for exposure settings as this led to brighter, well exposed and overall better quality images that required less processing. This is particularly apparent in the merging of images as it is possible to see each and every cell in both the green and red channels. The correct exposure also aided focus as the better exposed live images showed more clarity at the edges of cells.

Comparing the Well 1 images across all four experiments it is apparent that the indenter did make an impact to cell viability in the sample; in each case there was a high proportion of dead cells throughout the sample when the cells were loaded. Unfortunately, in Experiments 2 and 3 there were a lack of cells in the areas directly under the centre of the indenter. Experiment 4 strongly suggests that cell populations closer to the indenter centre (and therefore subjected to higher strains) have a higher death rate than cell populations further removed fro the point of impact. Experiment 1 could support this, however, as each of the recorded images is underneath the indenter there is a lack of information to show what happens beyond the indentation zone.

Experiments 2 and 3 provided less strong results but this was also a result of poorer, less densely populated cell samples in the observed areas. Certainly these two samples exhibited a high rate of cell death but arguably, there were not enough cells to observe for accurate results.

In all four experiments, the number of dead cells in the loaded samples is higher than that of the unloaded samples. Moreover, there seems to be a wider distribution (a more even distribution) of dead cells across the entire image sequences for the unloaded samples.

Looking at the images for Well 1 (Fig. 6.14) the initial images in steps 1 (6.14a) and 2 (6.14b) show that there are a high percentage of dead cells across the full sequence almost immediately. Between these steps, the cell viability remains fairly consistent but with an increase in the number of dead cells in the second image of the second step. In Fig. 6.14b the fourth image

is missing the red channel, a mistake when obtaining the data.

Two hours into the experiment and the cell viability has changed significantly (Fig. 6.14c). The changes are predominantly in the middling images (5-7).

Unfortunately, at the initiation point of step 4, some mechanical errors started to creep into the experiment; the motor stopped working at this point and the experiment had to be reset. This delayed the experiment by one or two minutes but the major problem was that the framed cells were now different to those that were initially being observed. Fig. 6.14d shows the images obtained for step 4. Although the cells in these images are not identical to those previously, the two sets were local to each other (likely within a millimetre) and the current cells were still directly under the indenter. This is to say that the new cell sample was still representative of the old sample and the results shouldn't instantly be dismissed.

During the third and fourth hours of testing the cell death numbers slowly increased across the full sample. The two channels don't line up perfectly for all images, which, can make the data harder to interpret but the clarity of the images shows a significant increase in the percentage of red cells across the range.

The final two hours of observation recorded a significant rise in the number of dead cells in the second and third images of the sequence. The first image appears to have a 100% dead cell rate and there are increases throughout the first half of the sequence. A similar pattern was observed as for all of the preceding images; a higher percentage of dead cells are observed in the areas closer to the centre of the indenter and there is a gradual decrease towards the furthest recorded point. Despite this decrease, there are sustained high numbers of dead cells noted across the full image sequence.
Overall it appears that over the six hours of testing there was a definite increase in the numbers of dead cells in the sample. Initially, there was a high percentage of dead cells particularly at the centre of the well, directly under the indenter. Over the next three hours, the cell viability steadily increased with a higher rate of cell death occurring through the middle of the sequence. This had the effect of having a more even cell viability distribution from images 1-7 in the sequence. In the last recorded hour of testing there seemed to be a large increase in the number of dead cells directly under the indenter area. In summary, it appears that the cell viability increased in the sample as the distance from the centre of the cell well (and indenter) increased.

In Well 2 there were a significant number of dead cells as soon as the experiment commenced, however, the distribution of the dead cells was quite different from that of Well 1 and the overall number was significantly less than that of the loaded cells. In Fig. (6.15a) it appears that there are a higher proportion of dead cells situated in images 5-9 of the image sequence. Whilst there appear to be many dead cells in the 5th and 6th images of the sequence, the overall count appears to be less than that obtained for the corresponding images from Well 1.

After two hours there seems to be little change in the cell viability across the whole sequence. In the third hour, as previously stated, the experiment had to be restarted. The first two images of the new sequence (Fig. 6.15d) have a high proportion of dead cells (similar to the corresponding images obtained for Well 1). Unlike Well 1, however, the cell viability remains almost constant throughout the next four hours.

Finally, Well 3 and the natural cells will be discussed. The was a high number of dead cells immediately in the well, albeit, less than the number of dead cells observed in the loaded sample. The overall distribution of the dead cells was fairly consistent across the whole image sequence. As the test continued the cell viability remained fairly consistent with little to no change observed across the entire five hours of testing.

In summary, more experiments will need to be undertaken with a full comparison to the strain states obtained by the numerical model. If more experiments can be conducted in a similar manor to Experiment 4 then it is possible that a large, quantifiable data set will be obtainable.

During this experiment it became apparent that the most important aspect of the results is the out of camera image. In order to obtain the highest quality images it is important that the exposures are correct at the time of capture. This reduces noise in the image, aids focusing and allows for simple post processing.
A final problem with some of the images related to the channels not lining up perfectly for each image. This could either be a result of an error in the platform control programme or it could be part of an issue which led to the breakdown of the microscope platform itself. The programme has been extensively tested and produced some good results but a further examination could locate a problem that was otherwise unnoticed. The platform is repairable, however, time constraints for the project meant that this was unachievable until after the writing of this thesis has been completed.

To improve the experiment, some new features should be introduced. Firstly, the environment should be changed or improved. Presently, there is no allowance for contaminant control during the experiment. This hasn't been a problem as of yet, however, in some results it is possible to see some particles in the cell samples (for example the last image in sequence Fig. 6.15d).

Full automation is also recommended, originally this was an objective of this thesis, however, it proved too difficult to accomplish due to problems of trying to programme for old equipment. It is likely that investing in new equipment would be the only way to develop a fully automatic experiment. If this was not an option, an autofocus system, auto-shutter system and auto-filter change system would need to be developed. This would require significant hardware addition, software development for each new piece of hardware and implementation into the current in-house control programme.

Presently; it is thought that if images could consistently be obtained to the quality of Experiment 4, and that the red and green channel images could be consistently well aligned; then it should be possible to use automatic analysis methods as documented in Section 6.3.

Chapter 7

Discussion and Conclusion

7.1 Discussion

The ultimate aim of this project is to develop a mechanical failure criterion for living human tissue. It is believed that the work completed during this thesis has significantly pushed the project closer to achieving this aim.
Throughout this thesis; theory, literature and experimentation have been used to investigate the effects of loading on cell viability, whilst, at the same time attempting to provide a foundation on which a mechanical failure criterion could be derived.

Four experiments have been completed and have provided data to show that mechanical loading has a significant impact on cell viability. Moreover, the fourth experiment provided some evidence to suggest that a function could be determined to relate cell death to strain.

The experimental process itself has been greatly developed since the previous cell deformation studies were undertaken by previous Aalborg University Alumni [Rasmussen, 2013], [da Silva Ferreira, 2014]. This development was aided by the implementation of the 'in-house' platform control programme, which, was created by [Gibson, 2016] and was further modified for use in this thesis. The ability to consistently capture image sequences increases the repeatability of the experiment and subsequently enables the possibility of observing the effects of strains over relatively large areas. Previously, it had not been possible to obtain such a quantity of data efficiently.

Unfortunately, the acquired results failed to meet the potential of the experiment. The first three experiments produced poor results due to a lack of experience of capturing fluorescent cell images. The fourth experiment signalled the beginning of a new set of experiments; lessons had been learnt from previous experiments and everything was in place to obtain high quality data. Unfortunately, this experiment had to conclude early due to a mechanical failure that also postponed any further testing.

Overall, the images did seem to suggest that the loaded cells had a higher rate of cell viability than the unloaded cell samples. The images obtained in Experiment 4 (Figs. 6.14, 6.15 and 6.16), also suggested that the cell populations located closer to the centre of the indenter died quicker than cell populations further from the point of highest strain. Many more experiments would need to be undertaken to investigate if this was the case or not, however, these tests did provided evidence that supported the hypothesis that cell death could be accelerated by applying strains.

To investigate this further, a quantifiable data set would need to be obtained where the cell viability in the samples was accurately and properly recorded for all experiments. Ideally, this would be accomplished using automatic counting methods such as those discussed in Section 6.3. It is possible that some of the data obtained in Experiment 4 could already be analysed accurately using the automatic cell counting processes available in ImageJ, however, time limitations restricted the possibility of testing this. The images could be tested as part of a further work strategy, however, regardless of whether any of the obtained data could be processed computationally or not, the images do show that the experimental set-up could consistently produce exceptional images by incorporating some small refinements.

It was shown that by using the live histogram available in Micro-manager 1.4, it is possible to capture images with great clarity and brightness. Thus, the quality of merged colour composite images is dependent on the overlapping of the two image channels. In some of the obtained images, the cells are perfectly merged, however, sometimes there is a distance between the two images. The cause of this needs to be determined. It could either be a software issue or a mechanical issue and this will need to be investigated. One of the motor drive screws on the microscope platform disconnected in the final experiment, which, thus rendered the platform useless until it can be repaired. Reassembling the drive screw may fix the problem, as it may have been loose throughout the experiments. Fixing this could provide images with sufficiently good quality for auto analysis but this will be investigated as further work.

Regardless of whether the images can be analysed automatically or not, the project requires that quantifiable cell counting is related to strain. In order to establish a quantifiable relationship between strain state and the rate of change of cell viability, it will be necessary to implement the numerical model. Originally, it was hoped that the numerical model would be applied in this thesis, however, due to numerous problems with the practical experiment, and a misguided attempt to fully automate the experiment, there was too little time to make use of it.

When implemented, the strain states calculated by the numerical model would be extrapolated to the acquired images. It would then be possible to identify the cell viability within different strain regions.

The FE model should be updated with improved material parameters. Presently, the material parameters are based on tensile tests performed on the alginate gel by [Rasmussen, 2013], however, the gel is being compressed in the experiment. It is likely that the gel exhibits different behavioural responses in compression than when it is in tension. This means that a compression test should be devised to obtain material parameters for the gel and the numerical model should be updated with these new parameters. This could improve the accuracy of the current model.

The primary weakness of the experiment is that it is still predominantly a manual experiment. An engineer conducting the experiment is required to capture each image, control the microscope shutter and the illumination filters. This limits the possibilities of the experiment as a twenty-four hour experiment with hourly time-steps becomes an overly demanding procedure for the engineer. This means that the experiment should be automated. This may be difficult to achieve with the current equipment as it would require the following:

- An autofocus motor and driver

- Automatic shutter control
- Automatic illumination filter changing
- Control programmes to control each of these

The alternative to this would be to update the experimental set-up.

At the present time, the project is in the intermediate phases of designing a mechanical failure criterion. The experiment is appropriate for establishing a relationship between strain and cell death and this is the fundamental starting point for developing a criterion. To achieve this aim, more data is required and better analysis methods need to be established. The priority should now be to integrate the FE model and to update the parameters; by achieving this, a quantifiable relationship between strain and cell death can be established and the project is one step closer to achieving the final aim.

7.2 Conclusion

This thesis documents the process for developing a mechanical failure criterion for living human tissue. An experimental test set-up was developed to investigate the effects of strain on cell viability. Four time-lapse experiments were undertaken to establish the effects of loading on the rate of change of cell viability. Three cell samples were observed in each experiment; one was subjected to loading and two were control samples. A layer of alginate gel was used to immobilise the loaded cells and to transfer the strains induced by loading. One control sample was used to investigate the effects of the alginate gel on the cells and the other was used to investigate the environmental effects. Data was obtained by acquiring microscopic image sequences of cells to investigate

Three of the four experiments provided images of poor quality due to a lack of experience in cell imaging. The fourth experiment provided images of excellent quality but was cut short due to a mechanical failure in the test-set up. Despite this, the results suggested that mechanical loading had a significant impact on cell death with cell samples exhibiting a faster rate of cell deterioration. The fourth experiment indicated that the rate of cell death was accelerated as strain levels increased.

In order to develop a mechanical failure criterion, more data is required. Most importantly, an existing numerical model needs to be updated and implemented so as to act as a reference for the strains induced with the loaded cell sample. This would establish a relationship between strain and cell viability, which would be the first step of establishing a mechanical failure criterion.

Bibliography

G. Bennett, C. Dealey, and J. Posnett. The cost of pressure ulcer in the uk. *Age Ageing*, 2004. 3

Calijn V. C. Bouten, Martin M, Knight, David A. Lee, and Daniel L. Bader. Compressive defromation and damage of muscle cell subpopulations in a model system. *Annals of Biomedical Engineering*, 29:153–163, February 2001. 4

R. G. M. Breuls, C. V. C. Bouten, C. W. J. Oomens, D. L. Bader, and F. P. T. Baaijens. Compression induced cell damage in engineered muscle tissue: An in vitro model to study pressure ulcer ateiology. *Annals of Biomedical Engineering*, 31:1357 – 1364, August 2003. 4, 22

R.M. Christensen. The first failure criterion. http://www.failurecriteria.com/thefirstfailurec.html, Feb 2017a. Accessed: 2017-05-29. 15

R.M Christensen. How do mises and tresca fit in. http://www.failurecriteria.com/misescriteriontr.html, 2017b. 15

Marcelo da Silva Ferreira. The effect of mechanical loading on the viability of skeletal muscle cells. Master's thesis, Aalborg Universtiy, June 2014. 5, 7, 57

Donati and Paoletti. Material properties of alginates. *Alginate: Biology and Applications*, pages 1–53, 2009. 17

K.I. Draget, K. Ostgaard, and Olav Smidsod. Alginate-based solid media for plant tissue culture. *Applied Micobiology and Biotechnology*, 1989. 18

Clive L. Dym and Irving H. Shames. *Solid Mechanics A Varaiational Approach (Aug. Edn.)*. Springer, 2013. 10, 12

Debby Gawlitta, Wei Li, Cees W. J. Oomens, Frank P. T. Baaijens, Dan L. Bader, and Carlijn. V. C. Bouten. The relative contributions of compression and hypoxia to develpment of muscle tissue damage: An in vitro study. *Annals of Biomedical Engineering*, 35:273–284, November 2006. 4

A. Gefen, L. Cornelissen, D. Gawlitta, D. Bader, and C. Oomens. The free diffusion of macromolecules in tissue-engineered skeletal muscle subject to large compression strains. *J. Biomech*, 2008. 5

D. Gibson. Automation of experimental process for designing a mechanical fairlure criterion for living human tissue. Master's thesis, Aalborg University, 2016. 5, 7, 57

Gorin and Spencer. Excocellular alginic acid from azotobacter vinelandii. *Canadian Journal of Chemistry*, 44, 1966. 17

Govan, Fyfe, and Jarman. Isolation of alginate-producing mutants of pseudonmonas fouorescens, pseudomonas putida and pseudomonas mendocina. *Microbilogy*, 125, 1981. 17

T. Vanden Hoek, Z. Shao, C. Li, R. Zak, P. Schumacker, and L. Becker. Reperfusion injury on cardiac myocytes after simulated ischemia. *American Journal of Physiology*, 1996. 3

E. Leopold and A. Geffen. Changes in permeability of the plasma membrance of myoblasts to fluorescent dyes with different molecular masses under sustaind unisxial stretching. *Medical Engineering and Physics*, 2013. 5

S. Preibisch, S. Saalfeld, and P. Tomancak. Globally optimal stitching of tiled 3d microscopic image acquisitions. *Bionformatics*, 2009. 29

T.J. Rasmussen. 3d defromation design study of myoblast cells. Master's thesis, Aalborg University, June 2013. 5, 7, 19, 21, 22, 57, 58

Bernd H. A. Rehm. *Alginate: Biology and Applications*, volume 13. Springer, 2009. 17

N. Slomka and A. Gefen. Relationship between strain levels and permeability of the plasma membrane in statically stretched myoblasts. *Annals of Biomedical Engineering*, 2012. 5

N. Slomka and A. Grefen. Conofocal microscopy-based three-dimensional cell-specific modelling. *Journal of Biomechanics*, 2010. 4

Olav Smidsrod and Gudmond Skjaak-Brik. Alginate as immobilization matrix for cells. *Trends in Biotechnology*, 1990. 17